Microporous and Mesoporous Materials 360 (2023) 112732

Contents lists available at ScienceDirect

Microporous and Mesoporous Materials

journal homepage: www.elsevier.com/locate/micromeso

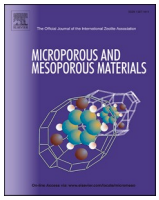

Hydroconversion of γ-valerolactone over Co/γ-Al_2O_3 and Co/H-Beta zeolite catalysts: Acidity and selectivity

Gyula Novodárszki [a], Ferenc Lónyi [a,*], Magdolna R. Mihályi [a], Anna Vikár [a], Róbert Barthos [a], Blanka Szabó [a], Jenő Hancsók [b], József Valyon [a], Hanna E. Solt [a]

[a] Research Centre for Natural Sciences, Institute of Materials and Environmental Chemistry, Renewable Energy Research Group, H-1117, Budapest, Magyar tudósok körútja 2, Hungary

[b] Research Centre for Biochemical, Environmental and Chemical Engineering, MOL Department of Hydrocarbon and Coal Processing, University of Pannonia, H-8200, Veszprém, Egyetem utca 10., Hungary

ARTICLE INFO

Keywords:
GVL hydroconversion
Co/γ-Al_2O_3
Co/H-Beta
2-MTHF
Pentanoic acid
DRIFTS-MS

ABSTRACT

Hydroconversion is an obvious way to convert γ-valerolactone (GVL) into value-added products. Co/γ-Al_2O_3 and Co/H-Beta catalysts were found to direct the reaction to get selectively 2-methyltetrahydrofuran (2-MTHF) and pentanoic acid (PA), respectively, at 200–250 °C. The activity difference were related to the difference of acid-base properties of the catalysts. Acid sites of the catalysts initiated opening of the [CH_3CH-O] bond of GVL well below 100 °C resulting in surface pentanoates (POAs). POA, strongly bound to Co/γ-Al_2O_3 was not converted to PA up to about 250 °C, but at ≥150 °C formation of 2-MTHF was initiated by reduction of the carbonyl group, hydrogenolysis of the obtained [O-COH] bond to 1,4-pentanediol, and dehydrocyclization. Formation of 2-MTHF prevailed up to about 250 °C, where conversion of POA to PA became accelerated. Over Co/H-Beta the reactions bringing about 2-MTHF could not compete with the facile conversion of GVL to PA.

1. Introduction

Converting lignocellulosic biomass into chemicals and fuels is of major interest because economy wants to reduce its dependence on fossil carbon resources. Biomass, particularly the non-food and non-feed lignocellulose is an abundant source of renewable carbon for the chemical industry. Levulinic acid (LA) is one of the most important platform chemicals, which is already produced from lignocellulose at industrial scale [1–3]. From LA γ-valerolactone (GVL) can be derived via consecutive catalytic dehydration and hydrogenation reactions [4–7]. GVL has the potential to be blended with gasoline [8,9], or to be used as commodity of alkenes, polymers, and a number of value-added chemical products [1,10–17]. By catalytic GVL hydroconversion mainly 2-methyltetrahydrofuran (2-MTHF) and/or pentanoic acid (PA) is obtained. The reaction can be directed by applying catalyst and reaction conditions to favor the formation of one or the other product [4,18,19].

The 2-MTHF is a hydrophobic cyclic ether having relatively high energy density, octane number (>90), and miscibility (60 v/v%) with gasoline. It can also be used as solvent in many organic reactions [1,20]. The ester of PA can be also admixed with gasoline or diesel, depending on the kind of esterifying alcohol [18,21].

The 2-MTHF was suggested to form in three consecutive reactions [4,18,19]. The GVL carbonyl group was shown to be hydrogenated as the first reaction step, giving cyclic ester 2-hydroxy-5-methyltetrahydrofuran (2-OH-5-MTHF). The hydrogenolysis of the ester bond results in the formation of 1,4-pentanediol. 2-MTHF is obtained if cyclodehydration of 1,4-PD occurs [9,22].

In contrast to 2-MTHF formation, the hydrogenation is the second reaction on the consecutive reaction route of PA formation [1,18,19,23]. The reaction was shown to be initiated by acid-catalyzed cleavage of the [CH_3CH-O] bond of GVL to pentenoic acid (PE) [10,17–19,24,25]. On Brønsted acid sites the ring opening was suggested to proceed via protonated surface intermediate. The formed 3-PE and 4-PE can isomerize then to 2-PE [17,25]. The ring opening mechanism on Lewis acid catalysts, such as γ-Al_2O_3, is not clarified yet. In the presence of hydrogen and hydrogenation catalytic function PEs can become quickly saturated to PA. The possibility that the formation of PA could proceed via direct GVL hydrogenolysis was excluded [1,18,19,23].

From above short survey, it follows that the selectivity of the GVL hydroconversion reaction is controlled by the relative rates of the metal-

* Corresponding author.
E-mail address: lonyi.ferenc@ttk.hu (F. Lónyi).

https://doi.org/10.1016/j.micromeso.2023.112732
Received 29 May 2023; Received in revised form 5 July 2023; Accepted 11 July 2023
Available online 13 July 2023

catalyzed hydrogenation and the acid-catalyzed ring opening. The corresponding rate constants are in turn dependent on the balance of the metallic and acidic functions, as well as the applied reaction conditions. Over a large variety of bifunctional heterogeneous catalysts, having Brønsted acidity mainly PA was formed in the presence of hydrogen or hydrogen source [18,19,26–32]. In contrast, it was found that reaction pathways, leading either to PA or to 2-MTHF product could prevail over supported metal catalysts, having Lewis acidity. For example, a 5% Pd/γ-Al_2O_3 catalyst gave PA as main product [33], whereas 2-MTHF or its 1,4-PD precursor was the main product if alumina-supported Cu, or Ni-Cu catalyst was used [34–36]. It was suggested that a bifunctional catalyst, having low hydrogenation activity, e.g., due to low metal loading, can push the selectivity towards PA, whereas a catalyst of dominating hydrogenation activity, for instance a catalyst of high metal loading and relatively low acidity, can direct the reaction toward 2-MTHF formation [4,18,19,23].

The present study concerns the GVL hydroconversion activity of zeolite H-Beta and γ-Al_2O_3-supported Co catalysts. Though the acidic and hydrogenation functions of the catalysts were found to be hardly different, PA was formed over the Co/H-Beta catalyst with high selectivity, whereas 2-MTHF was selectively formed over the Co/γ-Al_2O_3 catalyst. It was shown that the initial product over each catalyst was PA. While over the Co/H-Beta catalyst PA remained the main product during the time of the catalytic examination, over the Co/γ-Al_2O_3 catalyst the 2-MTHF selectivity started to prevail after a short initial period. This study shows that the steady-state GVL hydroconversion activity of bifunctional catalysts is generated in the interaction of the catalyst, the reactants, and the products.

2. Experimental

2.1. Catalyst preparation

Cobalt catalysts supported on γ-Al_2O_3 (Ketjen CK 300, AkzoNobel) or zeolite H-Beta (VALFOR® CP, Si/Al = 12.5, PQ Corp.) were prepared.

The alumina-supported catalyst was prepared by wet impregnation. The γ-Al_2O_3 support was dried at 110 °C for 24 h, then 10.4 g of the dehydrated material was suspended in 60 ml of 0.26 M aqueous solution of cobalt nitrate. The water was slowly evaporated from the suspension, the solid was dried at 110 °C for 12 h, and finally calcined in air at 500 °C for 3 h. The thus obtained catalyst is referred to as Co/γ-Al_2O_3.

The zeolite-supported cobalt catalyst was prepared by solid-state reaction between the H-form of zeolite Beta and Co(II)-nitrate. The H-Beta zeolite (8.8 g, with a water content of 12.5 wt%) was thoroughly homogenized with a calculated amount of Co(II)-nitrate hexahydrate powder (3.16 g) in an agate mortar for 30 min. The mixture was then heated up in air at a rate of 10 °C·min^{-1} to 500 °C and kept at this temperature for 3 h. The heat treatment resulted in melting and penetration of the cobalt salt into the micropores of the zeolite, and in its thermal decomposition [37]. The thus prepared catalyst was shown to contain Co-oxide species on the outer surface of the zeolite crystallites, and inside the pores. Some protons of the H-Beta zeolite were also replaced by cobalt cations [37,38]. The obtained catalyst is referred to as Co/H-Beta.

2.2. Catalyst characterization

The Co content of the catalysts was determined by atomic absorption spectroscopy (Varian SpectrAA-20). The specific surface area (SSA) of the catalysts were determined from their nitrogen adsorption isotherms by the Brunauer-Emmett-Teller (BET) method. Samples were pre-treated at 250 °C under 10^{-6} mbar vacuum for 4 h and the isotherms were determined at −196 °C using an automatic, volumetric adsorption analyser (The "Surfer", Thermo-Fisher Scientific).

The metal oxide and/or metal phases formed on the supports were identified by X-ray powder diffraction (XRPD) measurements using a Philips PW 1810/3710 diffractometer equipped with a graphite monochromator (CuK_α radiation, λ = 1.5418 Å) and a type HT1200 Anton Paar high-temperature chamber. The XRPD patterns were measured in steps of 0.02° 2Θ and scan time of 5 s in each step, whereas the X-ray tube was set at 40 kV and 35 mA. Both the air-calcined (as prepared) and reduced samples were investigated. When the reduced catalyst was studied, the sample was heated up *in situ* in the Anton Paar chamber in H_2-flow of 50 cm^3·min^{-1} at a rate of 10 °C·min^{-1} from room temperature to 450 °C and was treated at this temperature for 1 h. The sample was cooled then to room temperature in H_2 flow and the XRPD pattern was recorded. For the identification of the crystalline phases card No. 42–1467 for Co_3O_4, 48–1719 for CoO, 15–806 for *fcc* Co^0, 5–727 for *hcp* Co^0, and 10–425 for γ-Al_2O_3 was used from the ICDD database. The phase composition was determined using the full profile fitting method.

Sample morphology was studied by an FEI Tecnai G2 20 X Twin transmission electron microscope (TEM) at a 200 kV accelerating voltage. Samples were drop-cast from distilled water suspension onto a copper mounted holey carbon film.

Reducibility of Co in the air-calcined catalysts was studied by temperature-programmed hydrogen reduction (H_2-TPR) measurements. About 100 mg of the catalyst was placed into a quartz reactor tube (4 mm ID), treated in a 30 cm^3·min^{-1} O_2-flow at 500 °C for 1 h, cooled to 40 °C, and flushed with N_2 for 10 min. The H_2-TPR measurement was initiated by switching to a 20 cm^3·min^{-1} flow of 10.0 vol% H_2/N_2 mixture and then ramping up the temperature to 800 °C at a rate of 10 °C·min^{-1}. The reactor effluent was passed through a trap cooled by liquid nitrogen (−196 °C) to remove water from the gas before it reaches the thermal conductivity detector (TCD). The rate of hydrogen consumption during the reduction process was recorded by monitoring and processing the TCD signal.

The acidity of the catalysts was characterized by the Fourier-transform infrared (FT-IR) spectra of adsorbed pyridine (Py) using a Nicolet 6700 spectrometer (Thermo Scientific). The used IR cell allowed in-situ treatment of the self-supported catalyst wafer in gas flow or static/dynamic vacuum. Spectra of wafers, having a "thickness" of about 5 mg·cm^{-2}, were collected in transmission mode averaging 32 scans at a resolution of 2 cm^{-1}.

Before Py adsorption, the catalyst support materials were treated at 450 °C by evacuation in a high vacuum (~10^{-6} mbar) for 1 h, whereas the Co-containing catalysts were reduced in H_2 at 450 °C prior evacuation. After recording its spectrum, the pre-treated sample was contacted with vapor of Py at 5.7 mbar and 200 °C for 30 min. The sample was then degassed by evacuation at 200 °C for 30 min and a new spectrum was recorded at room temperature. The difference spectrum, generated by subtracting the spectrum of the neat wafer from the spectrum of the Py-loaded wafer showed the spectrum of surface species obtained from Py adsorption. The concentration of Brønsted and Lewis acid sites was calculated from the integrated absorbance of the characteristic absorption bands at 1540 cm^{-1} (pyridinium-ion) and 1450 cm^{-1} (coordinately bound Py), using integrated molar extinction coefficients of 1.07 and 1.65 cm μmol^{-1}, respectively [39].

The electronic state of the cobalt in the reduced Co/γ-Al_2O_3 and Co/H-Beta catalysts was characterized by the FT-IR spectrum of surface species formed from adsorption of CO [40,41]. The CO adsorption experiments were carried out using the same apparatus and pre-treatment procedure as applied in the Py adsorption experiments. The only difference was that the reduced catalyst was cooled down to room temperature before it was contacted with CO gas at 5 mbar pressure for 10 min. Spectra were taken in the presence of CO gas in the cell and after the gas and weakly bound CO were removed by evacuation at room temperature for 30 min. The difference spectra reflected the spectrum of surface species formed from CO adsorption.

2.3. Catalytic measurements

The catalytic hydroconversion of GVL were carried out in a flow-

through, tubular, fixed-bed microreactor (12 mm ID). The GVL reactant was fed into the reactor by a high-pressure liquid pump (Gilson, Model 302), while the H_2 co-feed was controlled by mass flow controller (Aalborg). One gram of catalyst, having a particle size of 0.315–0.63 mm, was placed in the reactor in between two layers of quartz particles. Before the catalytic tests, the catalyst was reduced *in situ* in the reactor by an H_2 flow of 100 $cm^3 \cdot min^{-1}$ at 30 bar and 450 °C for 2 h. The catalytic experiments were carried out in the 200–275 °C temperature range and in the total pressure range of 1–30 bar. The pressure of the catalytic system was set using a back pressure regulator. The space time of the GVL reactant and the partial pressure of H_2 were varied between 0.1 and 1.0 $g_{cat} \cdot g_{GVL}^{-1} \cdot h$ and 3.5−27.6 bar, respectively. The reactor effluent was flowed through a water-cooled condenser to separate gas and liquid phases. Before the gas flow reached the back pressure regulator it had to pass through a trap, cooled by an acetone/dry ice bath. The gaseous products were analyzed using an on-line GC (Varian 3300) equipped with flame ionization detector (FID) and a 30 m long Supelco (alumina/chloride) capillary column. The hourly formed liquid product was collected and analyzed by GC-MS (Shimadzu QP2010 SE) applying a 30 m ZB-WAX PLUS capillary column.

2.4. DRIFTS studies

DRIFTS-MS was used to monitor the temperature-programmed GVL reaction over the supported Co-catalysts.

A Nicolet iS10 spectrometer (Thermo Scientific) was equipped with a flow-through reactor cell and a DiffuseIR mirror system (PIKE Technologies). The finely powdered catalyst sample (about 20 mg) was placed into the sample holder of the reactor cell. The cell design allowed to pass gas flow through the catalyst bed. Before running reaction in the cell, the catalyst was pre-treated in a 30 $cm^3 \cdot min^{-1}$ H_2 flow at 450 °C for 1 h and cooled to about 30 °C either in H_2 or in He flow. The reaction of GVL was initiated by switching the H_2 or He flow to a gas saturator, containing GVL at room temperature. The saturated gas contained 430 ppm GVL. The catalyst was contacted with the GVL/H_2 or GVL/He mixture for 10 min at about 30 °C then the reaction temperature was raised at a rate of 2 $°C \cdot min^{-1}$ up to 275 °C. A DRIFT spectrum was taken in 5 min intervals, i.e., in about 10 °C increments. The catalytic system was in transient state due to the continuously increasing reaction temperature. From each of the thus obtained spectrum, the spectrum, recorded at the corresponding temperature in H_2 or He flow, was subtracted. The contribution of the gas phase to the difference spectra proved to be negligible under the applied conditions. Therefore, the obtained spectra practically reflect the surface species formed (positive bands) or consumed (negative bands) during the adsorption and reaction of GVL on the catalyst surface.

3. Results

3.1. Catalyst characterization

Some chemical, structural, and surface properties of the catalysts are summarized in Table 1. The Co content of the catalysts was about the same. Nitrogen adsorption/desorption isotherms of the supports and the catalysts are shown in Fig. S1. The SSA of the Co catalyst was about 13–16% lower than that of the corresponding support. Also, the pore diameter of the Co/γ-Al_2O_3 catalyst was smaller than that of the γ-Al_2O_3 support.

3.2. X-ray powder diffraction

Fig. 1 presents the XRPD patterns of oxidized (*a,d*) and reduced fresh (*b,e*) and used (*c,f*) Co/H-Beta and Co/γ-Al_2O_3 catalysts. The intense reflection at $2\theta = 22.52°$ and the low intensity reflections at 21.54, 25.43, 27.14, 28.82, 29.67, 33.49 and 43.71° are characteristic of zeolite Beta (Fig. 1, *a-c*), whereas the broad lines at 37.6, 39.5 and 45.9° stem from the γ-alumina support (Fig. 1, *d-f*). The presence of the diffraction lines at 31.3, 36.9, 38.6, 44.8, 55.7, and 59.4° (Fig. 1, *a* and *d*) indicate that crystalline Co_3O_4 phase (ICDD 78–1970) is present in both catalyst samples calcined at 500 °C. It should be noted that on the Co/γ-Al_2O_3 catalyst the formation of cobalt-aluminate phases, such as, $CoAl_2O_4$ (ICDD 82–2248) and Co_2AlO_4 (ICDD 38–0814) is also possible due to the diffusion of Co ions to the tetrahedral/octahedral sites of the γ-Al_2O_3 lattice during the calcination process. These phases cannot be distinguished from the Co_3O_4 phase by XRPD, because they all have a cubic spinel structure with almost identical diffraction pattern [42,43]. However, cobalt-aluminate phases represent hard-to-reduce Co species and therefore they can be distinguished from the Co_3O_4 phase by H_2-TPR method. Since no cobalt-aluminates could be detected by H_2-TPR (*vide infra*) the observed characteristic reflections in the XRPD patterns can be attributed to Co_3O_4 phase. (Nevertheless, the formation of a minor amount of Co-aluminate on the alumina surface without long-range order cannot be excluded.) The size of the Co_3O_4 particles in the calcined catalysts was determined from the $2\theta = 36.9°$ reflection using the Scherrer equation. Larger Co_3O_4 particles (~35 nm) were formed on the zeolite support, whereas smaller ones (~13 nm) on the γ-alumina.

In the *in situ* reduced catalysts, face-centered cubic (fcc) Co^0 was identified by the $2\theta = 44.2°$ and 51.5° reflections (Fig. 1, *b* and *e*). The XRPD pattern of Co/H-Beta catalyst indicate the presence of zero valent cobalt particles (Co^0) exclusively (Fig. 1, *b*). An average Co^0 diameter of 32 nm was calculated for Co/H-Beta by the Scherrer equation. In case of Co/γ-Al_2O_3, both fcc Co^0 and CoO (partially reduced Co_3O_4) phases were identified (Fig. 1, *e*). Because the main signal of fcc Co^0 phase was relatively weak and was overlapping with the broad line of the γ-alumina support, the support pattern was subtracted from the sample pattern and the difference diffractogram was evaluated to determine the average Co^0 particle size (Fig. S2). Phase analysis showed that about one

Table 1
Chemical, structural, and surface properties of supports and supported Co catalysts.

Support or Catalyst	Co content, wt%	SSA,[a] $m^2 \cdot g^{-1}$	Pore diameter,[b] nm	Reduction degree,[c] %	Average Co^0 diameter,[d] nm	Brønsted acid sites,[e] $mmol \cdot g^{-1}$	Lewis acid sites,[e] $mmol \cdot g^{-1}$
H-Beta	–	582	–	–	–	0.366	0.427
Co/H-Beta	7.2	508	–	65 (66)	32	0.122	0.457
γ-Al_2O_3	–	189	9.1	–	–	–	0.167
Co/γ-Al_2O_3	7.7	159	8.7	56 (98)	11	–	0.150

[a] The Specific Surface Area (SSA) was determined by the Brunauer-Emmett-Teller (BET) method.
[b] The most frequent pore diameter was calculated using the BJH method.
[c] The reduction degree at 450 °C or at 800 °C (in parenthesis) was calculated from the H_2-TPR curves.
[d] Calculated from the XRPD pattern of the catalysts reduced *in situ* at 450 °C for 1 h in H_2 flow.
[e] Determined by the FT-IR spectra of adsorbed pyridine. The concentration of Brønsted and Lewis acid sites was calculated from the integrated absorbance of the bands centered at 1540 and 1450 cm^{-1},respectively.

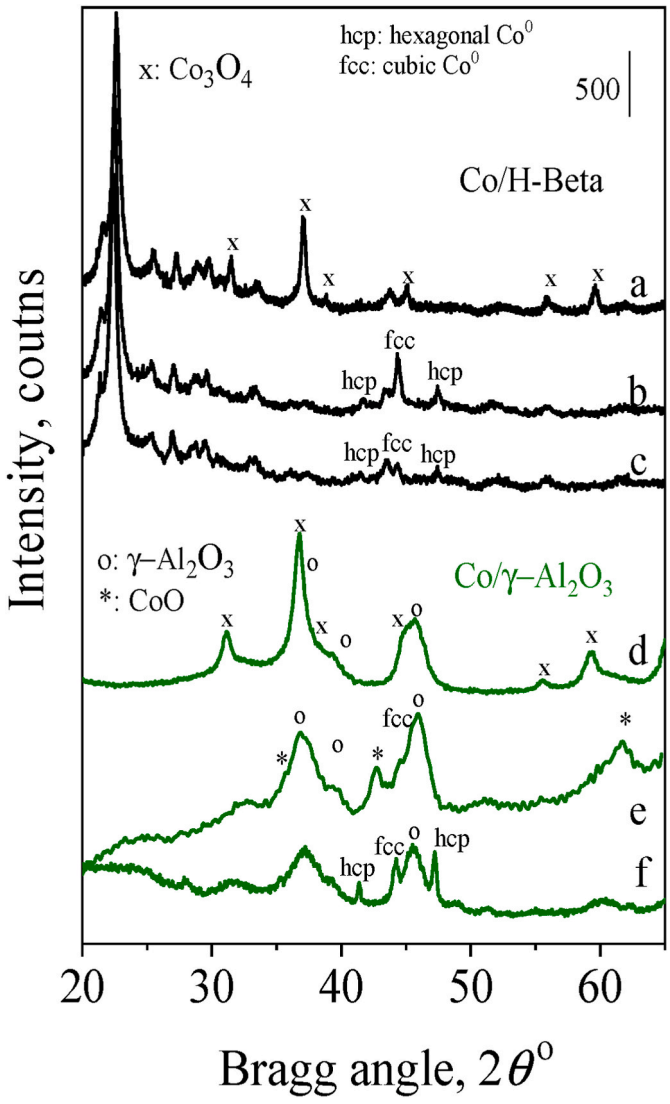

Fig. 1. XRPD patterns of the Co/H-Beta and Co/γ-Al_2O_3 catalysts: (a,d) air-calcined at 500 °C, (b,e) reduced *in situ* in the X-ray chamber at 450 °C in H_2 flow, (c,f) reduced *in situ* in the catalytic reactor and used for GVL hydro-conversion at 225 °C for 40 h time-on-stream.

third of the Co atoms was forming the Co^0 phase, having an average particle size of 11 nm. Accordingly, about two third of Co remained in partially reduced CoO form on the alumina surface as indicated by the diffraction lines at 2θ 42.4, 36.5, and 61.5°. (Fig. 1, *e* and Fig. S2). These findings are in line with former studies [44,45]. No diffraction lines of CoO could be identified in the diffractogram of the used Co/γ-Al_2O_3 catalyst (Fig. 1, *f*) indicating that the catalyst was further reduced during the catalytic run. Note that by the XRPD pattern of the *in situ* reduced Co/H-Beta, in addition to fcc Co^0 phase, a hexagonally close-packed (hcp) Co^0 phase was also identified. In the alumina-supported catalyst, however, such phase could be detected only in the used catalyst. Similar fcc-hpc phase transformation was already observed studying Co/SiO_2 catalyst [6].

The Co^0 particle size distributions shown on the TEM images of the catalysts (see Fig. S3) are in good agreement with those determined by XRPD method.

3.3. H_2-TPR

A previous H_2-TPR study [46] showed that Co_3O_4 particles, located on outer surface of zeolite crystallites, and CoO_x species dispersed within zeolite pores got reduced to Co^0 in the temperature ranges of about 200–400 °C and 400–600 °C, respectively. The reduction of Co^{2+} and $[Co\text{-}OH]^+$ lattice cations, balancing the negative zeolite framework charge, require reduction temperature higher than about 700 °C. In Fig. 2 H_2-TPR curves are shown for the Co/H-Beta and Co/γ-Al_2O_3 catalysts.

The Co/H-Beta exhibited a relatively sharp and high reduction peak in the temperature range of 200–450 °C having a maximum at 350 °C (Fig. 2A), whereas hydrogen consumption was negligible above 450 °C. These results suggested that Co_3O_4 phase was located on the outer surface of the zeolite crystallites in the Co/H-Beta catalyst (Fig. 2A). The H/Co atomic ratio, calculated from the hydrogen consumption up to 800 °C and the cobalt content of the catalyst, was 1.76. Considering that the full reduction of Co_3O_4 to metallic Co phase corresponds to an H/Co atomic ratio of 2.67, the average degree of Co reduction is 66%

(Table 1). Practically the same reduction degree could be reached by reducing the Co/H-Beta sample up to only 450 °C (cf. Fig. 2B1 and 2B2, Table 1). Note that XRPD detected only Co^0 in the reduced Co/H-Beta sample suggesting that the Co^0 fraction was practically equal with the reduction degree. The non-reducible cobalt can be cation of the zeolite lattice. The lattice cobalt cations are hard-to-reduce species because they are located in hard-to-access positions and/or far enough from each other to easily form Co–Co bonds [46].

In the TPR curve of the Co/γ-Al_2O_3 catalyst a sharp peak, centered at 320 °C appeared and a broad peak ranging from 350 up to 750 °C (Fig. 2A). There is no full consent in the interpretation of these peaks. The reduction of Co_3O_4 to Co^0 was considered as a two-step process ($Co_3O_4 + H_2 \rightarrow 3CoO + H_2O$ and $CoO + H_2 \rightarrow Co^0 + H_2O$). Accordingly, the first TPR peak was believed to indicate the reduction of Co_3O_4 to the intermediate CoO phase, whereas the second peak was presumed to stem from the reduction of CoO to Co^0 [47,48]. In contrast, others claimed that Co^0 was formed also in the first reduction step, whereas the broad high temperature TPR peak came from the reduction of Co-oxide species strongly interacting with the alumina surface [49,50]. Our results clearly favor this latter proposal, as we detected Co^0 species by XRPD in our Co/γ-Al_2O_3 sample reduced at 450 °C only (*vide supra*). Note that Co-aluminate, if present, gives a reduction peak only above 750 °C [44]. The TPR curve of the Co/γ-Al_2O_3 sample shows only a minor peak in the high-temperature range (Fig. 2A) indicating that no significant amount of Co-aluminate phase was formed. The H/Co atomic ratio, calculated from the hydrogen consumption up to 800 °C and the cobalt content of the catalyst was 2.61 suggesting a reduction degree of about 98% (Table 1). If the sample was reduced up to 450 °C only (Fig. 2B1) the H/Co ratio was 1.5 corresponding to average Co reduction degree of 56% (Table 1). The unreduced fraction is most probably CoO species, strongly interacting with the alumina surface (Fig. 2B2) [49,50]. The analysis of the XRPD pattern (Fig. S2) proved that Co^0 and CoO phase was present in the reduced sample in a molar ratio of about 1 to 2. Note that the reduction degree calculated from the H_2-TPR measurement is higher than the Co^0 fraction obtained from the XRPD analysis. Obviously, the partial reduction contributed to the reduction degree.

The catalyst was pre-reduced in H_2 flow at 450 °C *in situ* in the catalytic reactor before any catalytic run. Above results substantiate that in the thus activated Co/H-Beta catalyst about two third of the cobalt is in Co^0 state having an average Co^0 particle size of 32 nm. The similarly pre-treated Co/γ-Al_2O_3 catalyst contains about one third of the cobalt in Co^0 state having an average Co^0 particle size of 11 nm (Table 1). The unreduced fraction of Co is related to lattice Co-cations in the Co/H-Beta. In the Co/γ-Al_2O_3 catalyst, CoO strongly interacting with the alumina surface coexists with Co^0 particles.

3.4. *CO adsorption*

The FT-IR spectra of adsorbed CO characterizes the electronic state and environment of the sorption sites. Spectra of the studied catalysts were collected in the presence of CO gas in the FT-IR cell (Fig. 3, spectra

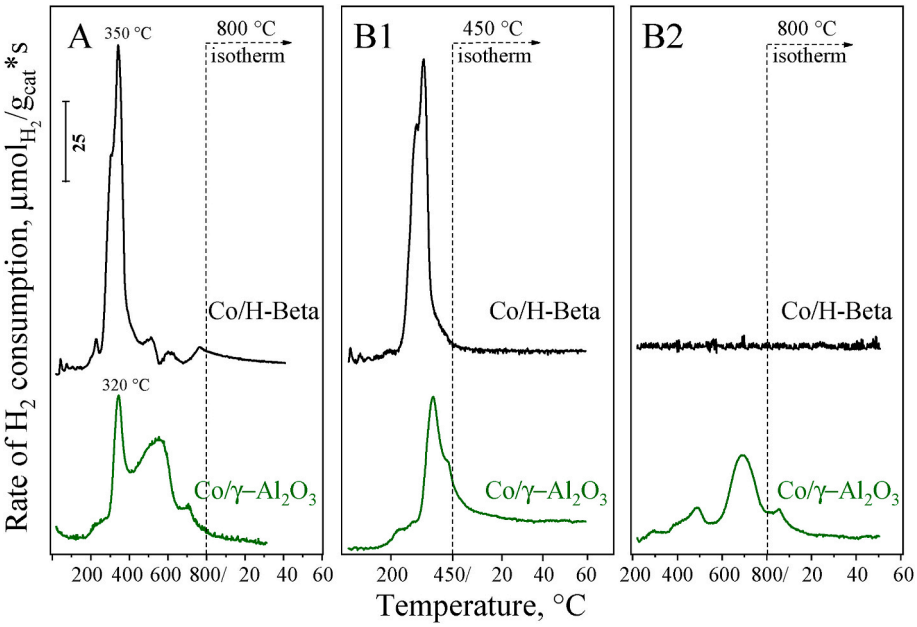

Fig. 2. H_2-TPR curves measured on the Co/H-Beta and Co/γ-Al_2O_3 catalysts. The samples were treated in O_2 flow (30 cm·min^{-1}) at 500 °C for 1 h, then cooled to 40 °C, purged with N_2 and heated up at a rate of 10 °C·min^{-1} to 800 °C in a flow of 9.0 vol% H_2/N_2 mixture (A). In a similar experiment, the samples were first heated to 450 °C and held at this temperature for 1h (B1), then cooled to 40 °C, and in the second step, the samples were again heated up to 800 °C (B2).

a) and after evacuation of the cell (Fig. 3, spectra *b*). In presence of CO gas relatively broad, overlapping bands appeared in the range of 2000–2070 cm^{-1} and above 2100 cm^{-1} (Fig. 3, spectra *a*). The bands of lower frequencies stem from CO bound to Co^0, whereas those above 2100 cm^{-1} belong to CO bound to cationic cobalt sites [41,51,52]. On Co^0 species CO can be adsorbed linearly as monocarbonyl, and also in the form of less stable multicarbonyls. In interaction with the support Co surface sites can carry partial positive or negative charge. This electronic state of the cobalt influences CO bonding that is reflected by the CO vibrational spectrum [41,51]. After evacuation practically a single band remained at about 2015 cm^{-1}, characteristic of Co^0-CO species.

The observation of Co^0-CO species proved that after H_2-reduction at 450 °C both catalysts contain Co^0 particles in comparable amounts. Co^0 particles are needed to activate hydrogen for the hydroconversion of GVL.

The bands above 2100 cm^{-1}, assigned to CO linearly adsorbed on Co^{n+} cations (n = 2, or 3) [41,51]. The cation coordinated carbonyls were stable only in the presence of CO gas in the IR cell and got removed easily by evacuation at room temperature (cf. Fig. 3, spectra *a* and *b*). The presence of the band at 2169 cm^{-1} in the spectrum of the alumina-supported Co catalyst indicates that the catalyst also contains unreduced Co-oxide phase, which is in accordance with our XRPD and TPR results (*vide supra*). The band at 2206 cm^{-1} in the spectrum of Co/H-Beta catalyst (Fig. 3) can be attributed to CO, linked to Co cations of the zeolite lattice [52].

3.5. FT-IR spectra of adsorbed pyridine

FT-IR spectra of Py adsorbed on the studied supported cobalt catalysts and their neat supports are shown in Fig. 4.

Pyridine, bound to Lewis acid sites only were detected on the γ-alumina support and the Co/γ-Al_2O_3 catalyst. The two pairs of bands at 1455/1624 and 1450/1617 cm^{-1} indicates two types of Lewis acid sites [53]. The Lewis acidity of γ-Al_2O_3 is undoubtedly comes from tri-coordinated surface Al^{3+} ions in coordinately unsaturated octahedral and tetrahedral sites [53]. The pair of bands at 1455/1624 cm^{-1} are due to Py bound to tetrahedral aluminum ions having a single coordinative unsaturation. These sites are considered to be the strongest Lewis acid sites, whereas the assignment of the other pair of bands at 1450/1617 cm^{-1} is still a matter of debate. Busca et al. [53] suggested that Py bounds also to Lewis acid sites of moderate acid strength. These sorption sites were substantiated to be pentacoordinated or tetracoordinated Al^{3+} ions, which are neighboring surface OH groups and are in singly and doubly unsaturated octahedral sites, respectively. In the Co/γ-Al_2O_3 the concentration of both type of Lewis sites are about 10% lower than in the γ-Al_2O_3 support (Fig. 4 and Table 1).

Pyridine adsorbed on the Brønsted sites of H-Beta gives the characteristic band pair at 1545/1637 cm^{-1} (Fig. 4) due to the 19b and 8a ring vibrational modes of protonated Py, respectively [39]. Beside the Brønsted acidity of bridging OH-groups, significant Lewis acidity was detected in the H-Beta zeolite (Table 1). Lewis acidity of zeolites are generally attributed to positively charged extra-framework alumina (e.g., AlO^+) species in the zeolite lattice. However, zeolite H-Beta may also contain significant amount of framework defect sites, wherein framework Al^{3+} atoms are linked to less than four [$SiO_{4/2}$] tetrahedra via oxygen atoms and behave as Lewis acid centers [54]. In the Co loaded sample the strength of the pyridinium bands at 1545/1637 cm^{-1} decreased significantly, indicating that about two-third of the lattice protons, i.e., Brønsted acid sites, were replaced by cations of cobalt (Fig. 4 and Table 1). Moreover, the intensity of the bands at 1455/1622 cm^{-1} was at least by 75% lower in the Co/H-Beta that it was in the H-Beta support. In the spectrum of the catalyst a similar, but somewhat shifted new pair of bands appeared at 1451/1611 cm^{-1} indicating that Lewis acid sites originally present in H-Beta were largely converted to a new type of Lewis acid sites, namely to Co cations occupying ion-exchange positions in the zeolite lattice [55].

The analysis of the ν_{OH} region on the H-Beta and Co/H-Beta samples clearly support the above notions (Fig. S4). The intensity of the ν_{OH} band, assigned to bridging OH groups (3610 cm^{-1}), is lower in the catalyst, confirming the exchange of protons by cobalt ions, such as, Co^{2+} or $Co[OH]^+$. The concentration of the Brønsted acid sites was by 0.244 mol·g^{-1} lower than that of the H-Beta (Table 1). Cobalt ions became also coordinated to framework Al defect sites terminating coordinative unsaturation and simultaneously generating new Lewis acid cobalt sites.

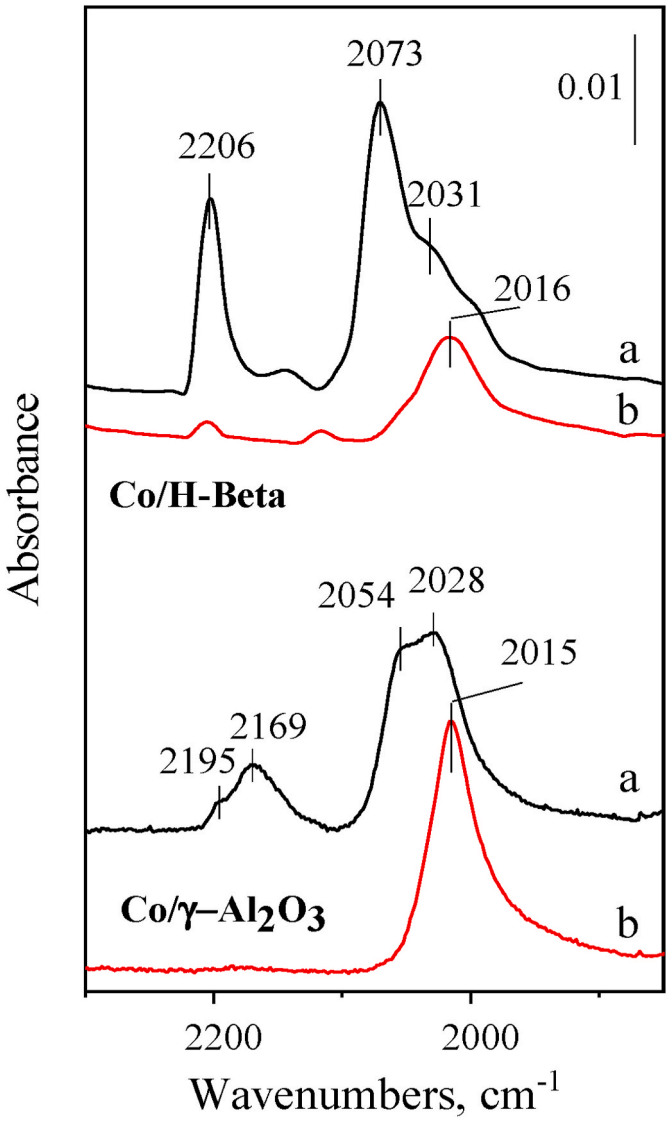

Fig. 3. FT-IR spectra of CO adsorbed on Co/H-Beta and Co/γ-Al_2O_3 reduced *in situ* in H_2 flow at 450 °C for 2 h. The catalyst sample was degassed after reduction by evacuation, cooled down to room temperature and contacted with CO at 5 mbar CO pressure for 10 min and spectrum (*a*) was recorded. The wafer was then evacuated in high vacuum for 10 min at room temperature, and spectrum (*b*) was recorded. Spectra are normalized to a wafer "thickness" of 5 mg cm^{-2}.

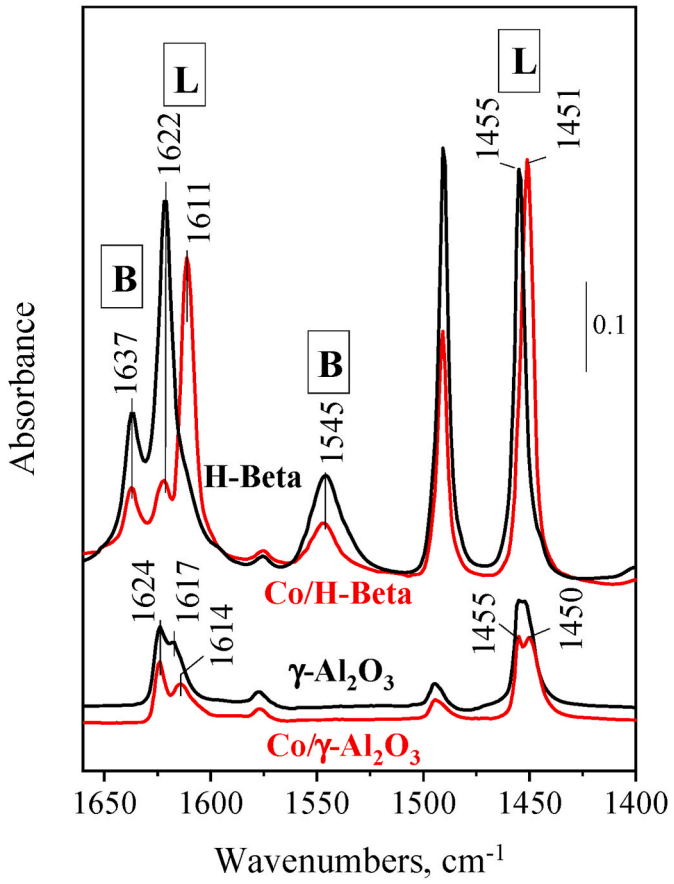

Fig. 4. FT-IR sepctra of adsorbed pyridine on activated H-Beta and γ-Al_2O_3 supports and reduced Co/H-Beta and Co/γ-Al_2O_3 catalysts. The supports were activated in high vacuum at 450 °C, whereas the Co catalysts were first reduced *in situ* in H_2 flow at 450 °C for 2h. Samples were contacted with pyridine vapor at 5 mbar and 200 °C for 30 min, then evacuated at this temperature for 30 min. The spectra were recorded at room temperature. L and B denotes characteristic bands of pyridine bound to Lewis or Brønsted acid centers, respectively. Spectra are normalized to a wafer "thickness" of 5 mg cm^{-2}.

3.6. Activity and selectivity

The GVL hydroconversion activity of the pure supports and the supported Co-catalysts was compared applying the same reaction conditions. While the reaction temperature or the space time was varied, the total pressure and the H_2/GVL molar ratio was fixed at 30 bar and 12, respectively. These conditions were selected because it was found that the pressure dependence of the conversion started to flatten at about 30 bar (Fig. S5).

Under hydrogen pressure but in absence of hydrogenation function, i.e., in absence of Co^0, only minor amounts of saturated products were obtained from GVL over the oxide supports. In line with the results of Wang et al. [25] the Lewis acid γ-alumina induced ring-opening of GVL, giving PE with selectivity as high as 94–96%, while under the applied reaction conditions the conversion was relatively low, 5–15% (Table S1). Under the same reaction conditions the PE selectivity of the H-Beta zeolite catalyst of strong Brønsted and Lewis acidity, was also as high as 76–86% but at somewhat higher conversion levels. The formation of butenes showed that the zeolite was also active in the decarboxylation of the primary product PE (Table S1). These results demonstrate that both Brønsted and Lewis acid sites can catalyze the cleavage of the [CH_3CH-O] bond of GVL.

Nearly full hydroconversion of GVL was reached at 225 °C over both supported cobalt catalysts; however, the main reaction product was different. The Co/H-Beta catalyst was highly selective for PA, whereas 2-MTHF was formed with high selectivity over the Co/γ-Al_2O_3 catalyst (Fig. 5, Table S2). The H-Beta zeolite induced the formation of unsaturated acid (PE) by cleaving the [CH_3CH-O] bond of the ring (Table S1). The Co/H-Beta catalyst, active in hydrogenation, gave saturated acid (PA). These findings suggest that the first step of the reaction was the same over the H-Beta support and the supported cobalt catalyst. However, the preferential formation of 2-MTHF suggests that an alternative reaction route prevails over the Co/γ-Al_2O_3 catalyst (Fig. 5, Table S2). We note here that a variety of catalysts used in former studies also showed diverse selectivities in the hydroconversion of GVL (Table S3).

The activity of the catalysts as a function of time-on-stream was also investigated (Fig. S6). Both the Co/H-Beta and Co/γ-Al_2O_3 catalysts showed high selectivity for PA and 2-MTHF products, respectively at high conversion level for at least 60 h on stream.

At higher reaction temperatures (>225 °C), minor products also appeared due to acceleration of side reactions (Fig. 5). Pentanoic acid pentylester (PPE), pentane, and 1-pentene formed over the Co/H-Beta

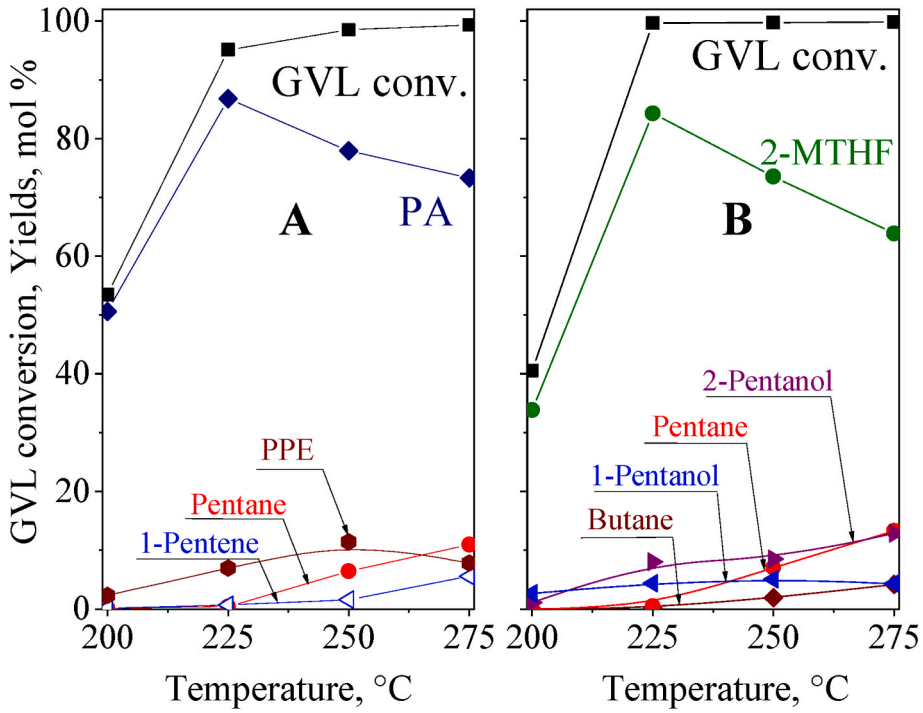

Fig. 5. GVL conversion and product yields over (A) Co/H-Beta and (B) Co/γ-Al_2O_3 catalysts as a function of reaction temperature at 30 bar and 1 $g_{cat.} \cdot g_{GVL}^{-1} \cdot h$ space time. The H_2/GVL molar ratio was 12. PA: pentanoic acid; PPE: pentanoic acid pentylester; 2-MTHF: 2-methyltetrahydrofuran.

catalyst (Fig. 5A), whereas pentanols, pentane, and butane side products appeared in the product mixture obtained on the Co/γ-Al_2O_3 catalyst (Fig. 5B).

GVL conversion and product yields were determined as the function of space time (Fig. 6). Over Co/H-Beta, minor amount of PE was formed at 200 °C (Fig. 6A). Its yield passed through a maximum, indicating that PE is an intermediate of PA. At 225 °C PE was not detected (Fig. 6A) because it was rapidly saturated to PA in a consecutive hydrogenation step. PPE was also formed in the reaction of PA with 1-pentanol. This latter intermediate must be the product of PA reduction. The 1-pentene and pentane had to be obtained from 1-pentanol (Fig. 6A). Obviously, the PPE yield decreases at higher space times because of the enhanced 1-pentanol dehydration/hydrogenation to pentane.

Over the Co/γ-Al_2O_3 catalyst, the formation 1,4-pentanediol (1,4-PD) is clearly discernible at 200 °C (Fig. 6B). The yield of 1,4-PD passes through a maximum, indicating that it is a possible intermediate of the 2-MTHF formation. It was shown earlier that formation of 2-MTHF proceeds in consecutive reaction through 2-OH-5-MTHF and 1,4-PD intermediates, which latter is converted to 2-MTHF by intramolecular cyclodehydration [19]. The 1-pentanol side product could be formed from 2-MTHF by the hydrogenolysis of the [CH_3CH-O] bond of the furan ring. Formation of 2-pentanol follows a similar pathway, but it is the [CH_2-O] bond that must break up (Fig. 6B). The origin of 2-butanol in the product mixture is less clear. This minor product might be formed from a non-detected intermediate via decarbonylation. The possible reaction routes leading to products and side products are summarized in Scheme S1.

3.7. DRIFTS reaction study

DRIFTS-MS was used to monitor the temperature-programmed reaction of GVL in He and H_2 gas flow over supported cobalt catalysts. The transient states of surface coverage and surface speciation was recorded as a function of temperature. Bands were assigned to group frequencies. These studies permitted to clarify the adsorption state of reactant GVL, provided information about the adsorbed intermediates and products, and made possible to draw conclusions about the route of transformations and the reaction mechanism.

3.7.1. Co/γ-Al_2O_3 catalyst

Upon contacting the Co/γ-Al_2O_3 catalyst with GVL/He flow development of negative absorption bands was observed in the difference spectra. The negative bands suggest that the GVL interacts via H-bonding to surface hydroxyl groups (Fig. S7A). The bands at 2980 and 2937 cm^{-1} (Fig. 7A) were assigned to $\nu_{as}[CH_3]$ and $\nu_{as}[CH_2]$ vibrations, respectively [56,57]. The band of relatively low intensity, discerned at 2878 cm^{-1} is attributed to $\nu_s[CH_3]$ vibration. Latter band partly overlaps with the $\nu_{as}[CH_2]$ band.

The carbonyl group of GVL gave three overlapping bands at 1767, 1742, and 1710 cm^{-1} (Fig. S8B, Fig. 7B). These bands are shifted downwards relatively to the carbonyl band of free GVL at 1782 cm^{-1}, suggesting the formation of adsorption complexes, having different strengths of interaction with the sorption sites. The stronger is the interaction between the GVL and the adsorption sites the lower is the carbonyl frequency [19,23,26,58].

In a recent study [19] we reported about carbonyl bands, obtained from adsorption of GVL on Co/SiO_2 catalyst and SiO_2 support. These bands were quite like those obtained from adsorption on the Co/γ-Al_2O_3 and the γ-Al_2O_3 support in the present study. Quantum chemical calculation suggested that these bands stemmed from three dominant adsorption complexes [19]. It seems very likely that the carbonyl bands of GVL bound to silica and alumina are similar because the modes of GVL co-ordinations to the adsorbing solids are also similar. The bands of deformation vibrations were assigned to $\beta_s[CH_2]$, $\delta_{as}[CH_3]$, $\beta_s[CH_2(C{=}O)]$, $\delta_s[CH_3]$, and $\delta[CH(O)]$ [19]. The above band assignments are summarized in Table 2.

It is important to note that very similar spectra were obtained from the adsorption of GVL on pure γ-Al_2O_3 support (Fig. S8) and Co/γ-Al_2O_3 catalyst (Fig. 7), suggesting that the adsorption sites are surface hydroxyl groups that are similar over these solids.

When the temperature of the system of catalyst/GVL/He flow was raised the intensity of the GVL bands decreased for two reasons: the

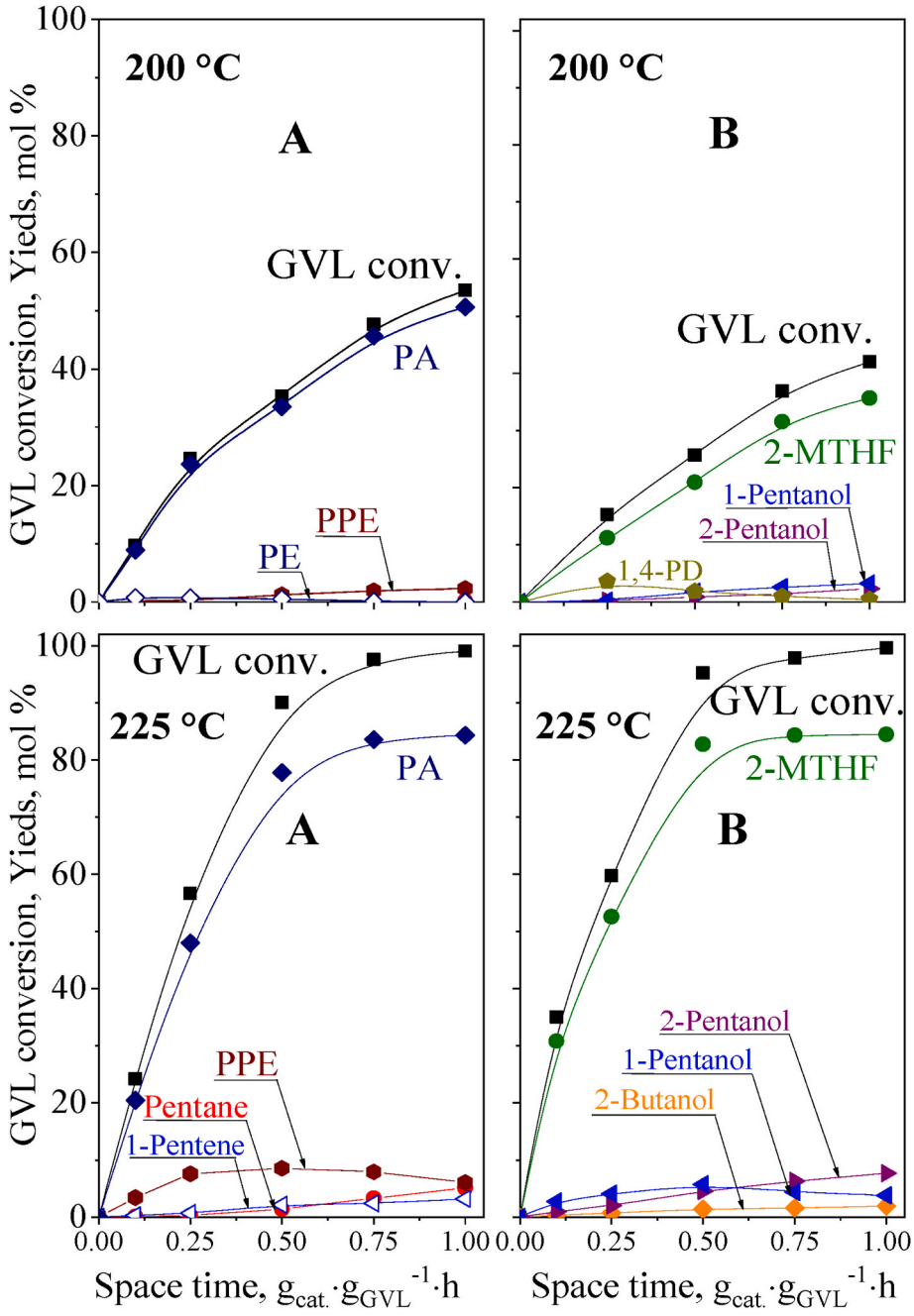

Fig. 6. GVL conversion and product yields over (A) Co/H-Beta and (B) Co/γ-Al_2O_3 catalysts as a function of space time at 200 °C and 225 °C. The total pressure was 30 bar, while the H_2/GVL molar ratio was 12. PA: pentanoic acid; PPE: pentanoic acid pentylester; 2-MTHF: 2-methyltetrahydrofuran.

decrease of adsorption coverage and the GVL conversions. The GVL conversions resulted in the generation of gaseous products and new surface species. The bands of C-H stretching vibrations shifted slightly, became broader and, most importantly, a new pair of bands appeared at 3085 and 3005 cm^{-1} (Fig. 7A and Fig. S8A). These new bands can be assigned to $\nu[=CH_2]$ and $\nu[=CH]$ vibrations [56,57], indicating the formation of a surface intermediate that contains terminal [CH_2=CH–] vinyl group. The corresponding ν[C=C] vibration band became discernible at 1642 cm^{-1} (Fig. 7B, Fig. S8B). The formation of vinyl group was accompanied by the development of overlapping broad features in the range of 1700-1300 cm^{-1}. The band pairs at 1580/1460 cm^{-1}, and 1650/1390 cm^{-1} (Fig. S8B) show close resemblance to the bands of surface carboxylates, obtained from PA adsorption over alumina [59]. Thus, the pair of bands at 1580/1460 cm^{-1} can be assigned to the asymmetric and symmetric vibrations of chelating bidentate surface carboxylate species, whereas the pair of bands at 1650/1390 cm^{-1} can be attributed to monodentate carboxylate species [59–63]. It is important to note that bidentate carboxylate species were formed in reaction with surface hydroxyl groups [60,61,64], whereas monodentate carboxylate species were formed over strong Lewis acid/Lewis base pair sites [59]. An additional pair of bands were also discernible at about 1610/1420 cm^{-1} (Fig. 7B). We associate latter bands with bidentate carboxylate species bound to Lewis acid/Lewis base (cobalt cation)/(oxide anion) pair sites of the catalyst (Table 3) [6]. Note that all of the surface-bound carboxylate species were thermally stable due to their strong interaction with the catalyst surface. The above-described changes of surface speciation, induced by raising temperature, strongly suggest that in absence of hydrogen the opening of

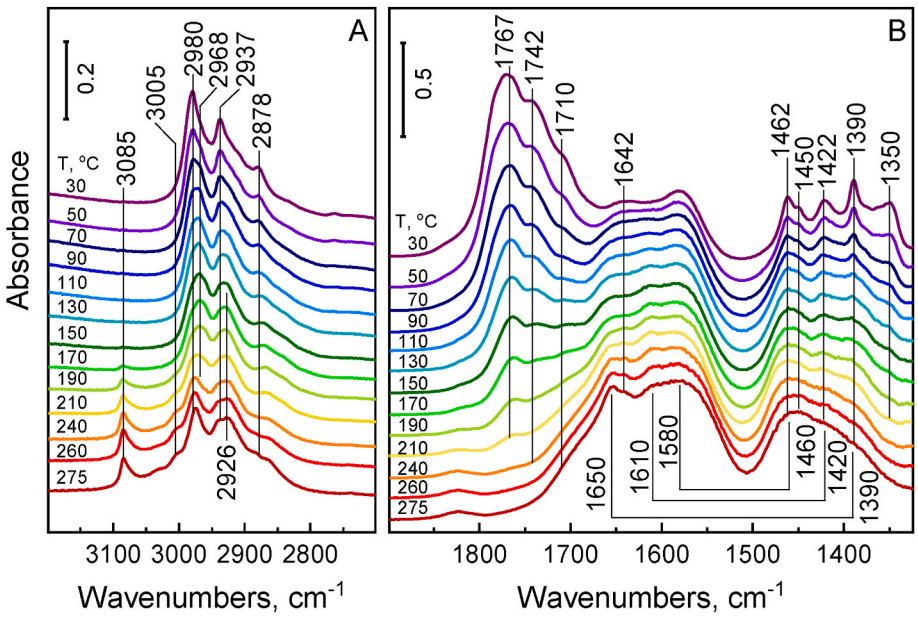

Fig. 7. DRIFT spectra of the species obtained from adsorption and reaction of GVL in He on Co/γ-Al_2O_3 catalyst in the frequency range of (A) the C-H stretching vibrations and (B) the carbonyl stretching and C-H deformation vibrations. The catalyst was contacted with a continuous flow of GVL/He atmospheric gas mixture, while the temperature was continuously raised at a rate of 2 °C·min^{-1} from 30 up to 275 °C. The corresponding spectrum of the neat catalyst was subtracted from the spectrum recorded at the indicated temperature.

Table 2
Characteristic absorption bands observed upon contacting Co/γ-Al_2O_3 and the γ-Al_2O_3 support with GVL/He at room temperature and their assignments.

Peak position, cm^{-1}	Assignment	Comment
2980	$\nu_{as}[CH_3]$	asymmetric stretching vibration of methyl group
2937	$\nu_{as}[CH_2]$	asymmetric stretching vibration of methylene group
2878	$\nu_s[CH_3]$	symmetric stretching vibration of methyl group
1767, 1742, 1710	ν[C=O]	carbonyl bands of GVL in three dominating adsorption complexes
1462	$\beta_s[CH_2]$	scissoring vibration of methylene group
1450	$\delta_{as}[CH_3]$	asymmetric vibration of methyl group
1422	$\beta_s[CH_2(C=O)]$	scissoring vibration of methylene group adjacent to the carbonyl group
1390	$\delta_s[CH_3]$	symmetric vibration of methyl group
1350	δ[CH(O)]	bending vibration of the methine group connected to the oxygen atom of the lactone ring

Table 3
New absorption bands developed at elevating temperature on Co/γ-Al_2O_3 or the γ-alumina support in contact with GVL/He and their assignments.

Peak position, cm^{-1}	Assignment	Comment
3085, 3005	$\nu[=CH_2]$, $\nu[=CH]$	stretching vibrations of a vinyl end group
1580, 1460	ν_{as}[O-C-O], ν_s[O-C-O]	asymmetric and symmetric stretching vibration of chelating bidentate carboxylate species formed on surface OH-groups
1650, 1390	ν_{as}[O-C-O], ν_s[O-C-O]	asymmetric and symmetric stretching vibration of monodentate carboxylate species formed on Lewis acid/Lewis base pair sites of γ-Al_2O_3
1610, 1420	ν_{as}[O-C-O], ν_s[O-C-O]	asymmetric and symmetric stretching vibration of bidentate carboxylate species formed on Lewis acid/Lewis base cobalt cation/oxide anion pair site

GVL ring proceeds on Lewis acid sites by cleavage of the [CH_3CH-O] bond and results in the formation 4-PE (Table S1), as well as, strongly bonded, vinyl-group-containing surface pentenoate (4-POE) species.

In presence of hydrogen the main product of GVL conversion was 2-MTHF over Co/γ-Al_2O_3 catalyst above about 200 °C (Figs. 5 and 6). The spectra obtained for the Co/γ-.Al_2O_3 catalyst in contact with GVL/H_2 flow show close resemblance to those obtained from the contact of the same catalyst with GVL/He flow (cf. Figs. 7 and 8), however, there are some distinct differences. The absorption bands of GVL become weaker when the temperature is increased because the adsorption coverage is decreased. Also, the formation of gaseous products, mainly 2-MTHF, and new adsorption intermediates contributed to the decrease of GVL coverage. Like from the GVL/He flow the spectra obtained from the GVL/H_2 flow showed formation of surface carboxylate species, but the vinyl bands were missing (cf. bottom spectra in Figs. 7 and 8). These results suggested that the same surface reactions occurred in H_2 and He, except that the presence of hydrogen and cobalt promoted the formation surface pentanoate and pentanoic acid, POA and PA. Strongly-bound surface carboxylates are formed in reaction with surface OH-groups and Lewis acid/Lewis base pair sites. In GVL/H_2 flow the intensity of the pair bands of monodentate carboxylate species at 1650/1390 cm^{-1} start to decrease above about 250 °C (Fig. 8B), suggesting that these species participate in further surface transformation and/or become converted to gaseous products. Parallel product and surface analysis suggested that annihilation of monodentate surface carboxylates was associated with PA formation (Fig. S9A).

Note that carboxylates are accumulated over the Co/γ-Al_2O_3 catalyst surface during the GVL reaction both in He and H_2 carrier gas but the conversion in H_2 resulted in the formation of 2-MTHF as main product (Fig. 5B, Table S2), as evidenced also by its MS detection (Fig. S9). These

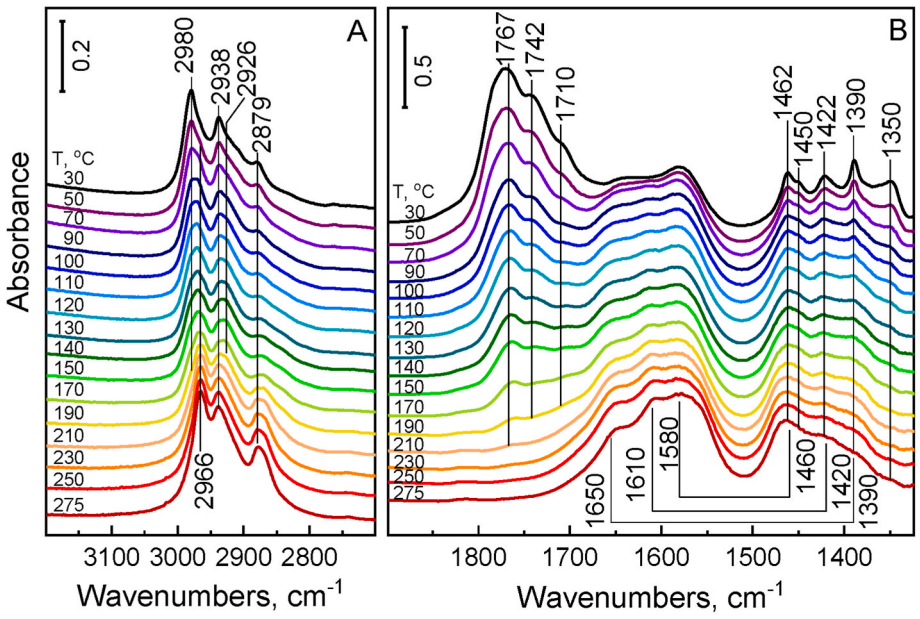

Fig. 8. DRIFT spectra of the species obtained from adsorption and reaction of GVL in H_2 on Co/γ-Al_2O_3 catalyst in the frequency range of (A) the C-H stretching vibrations and (B) the carbonyl stretching and C-H deformation vibrations. The catalyst was contacted with a continuous flow of GVL/H_2 atmospheric gas mixture, while the temperature was continuously raised at a rate of 2 °C·min^{-1} from 30 up to 275 °C. The corresponding spectrum of the neat catalyst was subtracted from the spectrum recorded at the indicated temperature.

results tell us that a reaction route other than the formation of surface carboxylates and carboxylic acid prevails in the presence of cobalt and hydrogen. The analysis of the C-H deformation bands (Fig. S10) permitted to clarify the reaction route, leading to 2-MTHF formation.

When the reaction temperature was linearly increased the intensity of the δ[CH(O)] band decreased more rapidly than that of the β_s[CH_2(C=O)] band, suggesting that the bands lost intensity not only due to GVL desorption, which would affect all the bands to the same extent, but also because GVL transformations. The [CH_3CH-O] bond cleavage, resulting in POE formation in He and POA formation in H_2, had a stronger response to the temperature raising than those reactions which eliminated the GVL carbonyl group (Fig. S10).

It is worth to compare the temperature dependence of the above discussed bands also in GVL/He and GVL/H_2 flows. The less pronounced drop of the δ_s[CH_3] in H_2 is in line with POA formation and the preservation of the [CH_3] end group. However, as temperature was increased the intensity of the β_s[CH_2(C=O)] band decreased more in hydrogen than in He (Fig. S10) implying that besides GVL desorption and [CH_3CH-O] bond cleavage the hydrogenation of the carbonyl group also prevails. The less pronounced drop of δ[CH(O)] band in hydrogen is in line with this latter reaction also suggesting that the reduction of the carbonyl group and the subsequent 2-MTHF formation competes with [CH_3CH-O] bond cleavage. Above results substantiate that two parallel surface reactions proceed on the Co/γ-Al_2O_3 catalyst in H_2: accumulation of POA species on the catalyst surface and hydrogenation of the carbonyl group of GVL. PA is formed from the monodentate pentanoate species, strongly bound to Lewis acid/Lewis base pair sites of alumina, only above about 250 °C (Fig. S9). Hydrogenation of GVL carbonyl must result in the formation of 2-OH-5-MTHF. Because no 2-OH-5-MTHF was detected in the product mixture it must be a surface-bound intermediate that is rapidly converted to other products, such as 1,4-PD that is an intermediate of the main product 2-MTHF formation. The 2-MTHF was found to be the main product of the GVL hydroconversion over Co/γ-Al_2O_3 catalyst (Fig. 5B, Fig. S9).

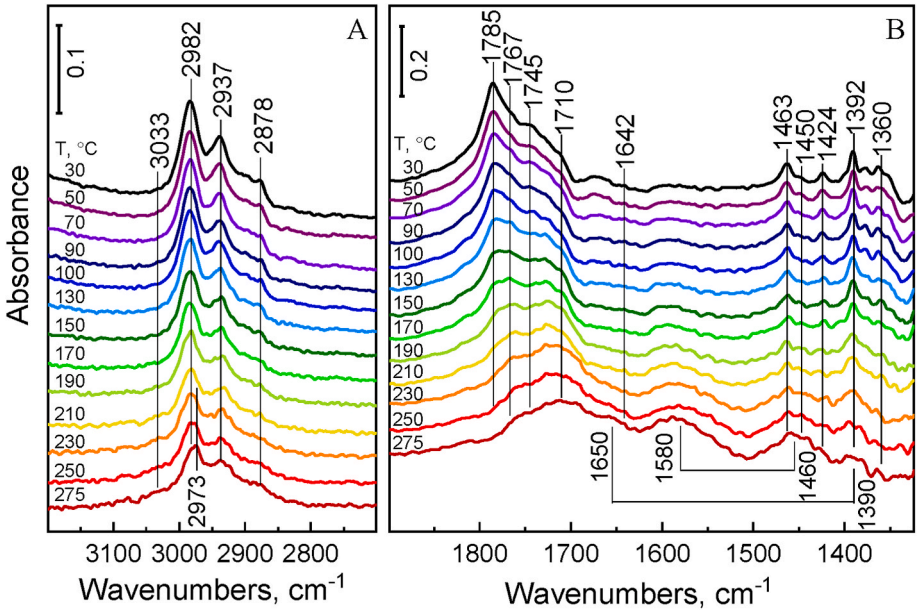

Fig. 9. DRIFT spectra of the species obtained from adsorption and reaction of GVL in He on Co/H-Beta catalyst in the frequency range of (A) the C-H stretching vibrations and (B) the carbonyl stretching and C-H deformation vibrations. The catalyst was contacted with a continuous flow of GVL/He atmospheric gas mixture, while the temperature was continuously raised at a rate of 2 °C·min^{-1} from 30 up to 275 °C. The corresponding spectrum of the neat catalyst was subtracted from the spectrum recorded at the indicated temperature.

3.7.2. Co/H-Beta catalyst

The formation of adsorbed species on the activated Co/H-Beta catalyst in contact with GVL/He at room temperature (Fig. 9) was accompanied by the development of negative absorption bands in the range of the ν_{OH} stretching vibrations (Fig. S7B) suggesting that GVL interacts via H-bonding to different types of surface hydroxyl groups including non-acidic and acidic hydroxyl groups of zeolite H-Beta. The spectra of Co/H-Beta and Co/γ-Al_2O_3 catalysts showed practically the same characteristic absorption bands (Table 2), except that an additional carbonyl band appeared near to the frequency of free GVL at 1785 cm^{-1} (cf. Figs. 9 and 7, top spectra).

At elevated temperatures some C-H stretching bands showed slight red shift (Fig. 9A). No distinct pair of bands appeared in the 3000-3100 cm^{-1} wavenumber region, where bands of ν[=CH_2] and ν[=CH] vibrational transitions were expected to appear due to brake of the [CH_3CH-O] bond and formation of vinyl group above about 200 °C temperature. The ν[=CH] vibration of a [-CH=CH-] group was expected to appear at about 3033 cm^{-1} [56,57]. The band at 3033 cm^{-1} is clearly seen in the spectra, obtained from adsorption of GVL on H-Beta above about 150 °C (Fig. S11A). A band like this can indicate surface reaction leading to the formation of a surface intermediate with an unsaturation along the carbon chain (Fig. 9A). The corresponding ν[C=C] vibration is discernible at 1642 cm^{-1} (Fig. 9B and Fig. S11B). The formation of –CH=CH– group was accompanied by the development of overlapping broad features in the spectral range of 1700-1300 cm^{-1} (Fig. 9B and Fig. S11B). The assignment of these bands is the same as was for the corresponding bands of species formed on alumina, namely, bands of bidentate (pair of bands at 1580/1460 cm^{-1}) and monodentate (pair of bands at 1650/1390 cm^{-1}) carboxylate species, respectively (Table 3). These results strongly suggest that the acid sites of H-Beta or Co/H-Beta induces opening the lactone ring by breaking the [CH_3CH-O] bond resulting in the formation of 3- or 2-PE and strongly bonded surface POE species.

The formation of carboxylates on H-Beta needs some explanation. Since carboxylate formation requires Lewis acid/Lewis base pair sites or basic OH-groups, the surface carboxylates were most probably formed with the involvement of extra framework aluminum species and coordinately unsaturated aluminum atoms, both present in zeolite H-Beta (Fig. 4 and Table 1). Formation of carboxylate with involvement of proton donor Brønsted acid sites is improbable.

The carboxylate bands of Co/H-Beta catalyst were much weaker than those of the H-Beta support (cf. Fig. 9B and Fig. S11). This can be explained by the partial elimination and/or transformation of the extra framework species in the process of Co introduction in the zeolite (see Fig. S4 and Fig. 4). Note that unlike to Co/γ-Al_2O_3 catalyst, no cobalt-oxide-bound carboxylate species were formed on Co/H-Beta, since latter catalyst contained only Co^0 particles and lattice Co-cations. (Fig. 2 and Table 1).

The spectra collected for the Co/H-Beta in contact with GVL/H_2 flow were similar to those obtained in GVL/He flow (cf. Figs. 9 and 10), except that the ν[=CH] band in the 3000-3100 cm^{-1} range did not appear. It follows that the ring opening of GVL, and formation of carboxylate species occur both in H_2 and He; however, in the presence of hydrogen and cobalt metal the formation of saturated carboxylate a carboxylic acid, namely PA, is favored.

The conversion of GVL over zeolite H-Beta resulted in the formation of PE (Table S1), whereas its hydroconversion over Co/H-Beta catalyst gave either PA or 2-MTHF as main product, depending on the reaction temperature (Fig. 5A, Fig. S12). Hydroconversion of GVL to 2-MTHF started already at temperatures above about 100 °C, reached maximum rate at about 150 °C, and declined near to zero over about 170 °C, where on the other hand the formation rate of PA got accelerated (Fig. S12). Note that formation of 2-MTHF started also at about 100 °C over the Co/γ-Al_2O_3 catalyst, but it began to decline at significantly higher temperatures than over the Co/H-Beta catalyst (cf. Fig. S9 and Fig. S12).

The analysis of the C-H deformation bands (Fig. S13) is in agreement with the above results. When the temperature was raised the strength of the β_s[CH_2(C=O)] band showed somewhat more pronounced decrease in H_2 than in He suggesting that the hydrogenation of the carbonyl group, introducing the formation of 2-MTHF also occurs in the 30–160 °C temperature range. Furthermore, the intensity of the δ[CH(O)] band decreased more quickly than that of any other characteristic bands (Fig. S13, indicating that the ring braking at the [CH_3CH-O] bond, introducing PA formation, is the preferred transformation on the surface (Fig. S12). Over Co/H-Beta the PA formation dominates above about 200 °C, where the rate of Brønsted acid-initiated ring opening reaction significantly exceeds the rate of cobalt initiated carbonyl hydrogenation, which latter is the first step towards 2-MTHF formation.

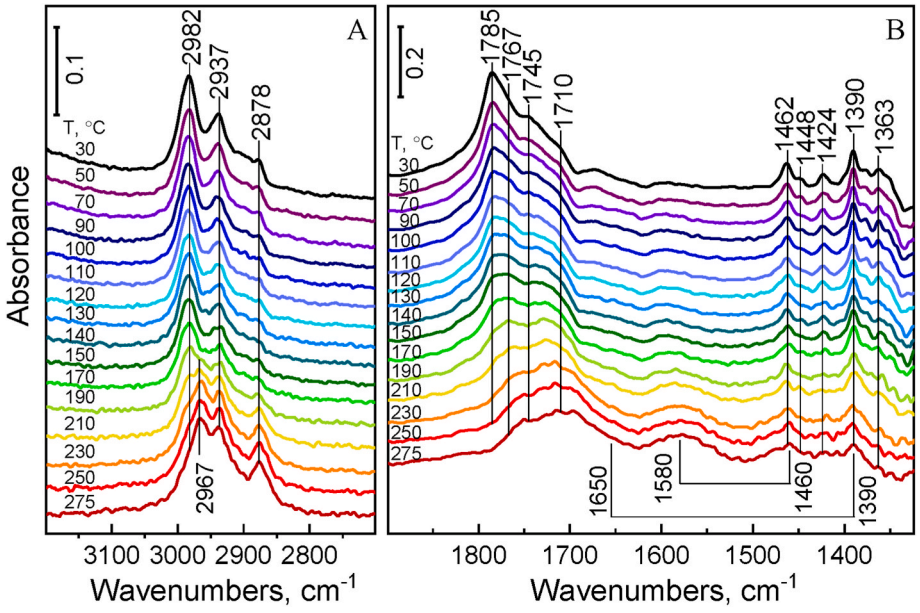

Fig. 10. DRIFT spectra of the species obtained from adsorption and reaction of GVL in H_2 on Co/H-Beta catalyst in the frequency range of (A) the C-H stretching vibrations and (B) the carbonyl stretching and C-H deformation vibrations. The catalyst was contacted with a continuous flow of GVL/H_2 atmospheric gas mixture, while the temperature was continuously raised at a rate of 2 °C·min^{-1} from 30 up to 275 °C. The corresponding spectrum of the neat catalyst was subtracted from the spectrum recorded at the indicated temperature.

4. Discussion

4.1. Acidity and activity

The spectra obtained from adsorption of Py showed that the γ-Al_2O_3 support contains solely Lewis acid sites, whereas both Brønsted and Lewis acid sites are present in the zeolite H-Beta support. The introduction of cobalt hardly influenced the acidity of the alumina (Fig. 4, Table 1). In contrast, zeolite protons became exchanged for cobalt cations and a large fraction (>75%) of the Lewis acid extra-framework alumina species and framework Al defect sites was replaced by new Lewis acid cobalt species (Fig. 4 and Table 1). Nevertheless, still about one third of the Brønsted acid bridged hydroxyl groups of the zeolite remained unaffected.

The Co/γ-Al_2O_3 and Co/H-Beta catalysts had about the same Co content (Table 1). Reduction of the catalyst precursors resulted in the formation of zero-valent cobalt particles (Co^0) in both catalysts, although a considerable fraction of cobalt remained in not fully reduced form (Fig. 2 and Table 1). In the Co/γ-Al_2O_3 catalyst, about one third of the Co content is in Co^0 state, whereas about two third is present as CoO, strongly interacting with the alumina surface. In the Co/H-Beta catalyst, about two third of the cobalt content was transformed to Co^0 particles and the rest is present as lattice cation in the zeolite. The different adsorbed CO species confirmed the coexistence of different sorption site cobalt species in the catalysts (Fig. 3). The comparable infrared absorption intensity of linear Co^0-carbonyls, obtained from CO adsorption showed that the metal surface, available for triggering hydrogenation/dehydrogenation reactions does not much differ in the two catalysts.

In agreement with former studies [10,17,18,25], both γ-Al_2O_3 and zeolite H-Beta showed reasonable activity in the ring opening of GVL to PE (Table S1). The zeolite H-Beta, containing not only Lewis but also Brønsted acid sites was more active than the purely Lewis acid γ-Al_2O_3 (Table S1).

On Brønsted acid sites the ring opening of GVL was suggested to proceed via protonated surface intermediate to produce 3- and 4-PE, which can isomerize to give 2-PE [17,25]. In the present study, the surface intermediate formed on Brønsted acid site contains unsaturation along the carbon chain suggesting the formation of a surface intermediate possibly leading to 3- or 2-PE product (Fig. S11). This observation suggests that the reaction proceeds likely as proposed in Scheme 1A. In the first step, a protonated adduct is formed with the involment of a Brønsted acid site, represented by H^+Z^-, where Z^- denotes the negatively charged zeolite framework, i.e. the conjugate base of the Brønsted acid protons. The protonated adduct is in equilibrium with carbenium ion intermediates. From the intermediate 2- or 3-pentenoic acid is formed, while the Brønsted acid site is regenerated.

The ring opening mechanism on Lewis acid γ-Al_2O_3 has not been clarified yet. We have shown that the surface intermediate contains a vinyl group (Fig. S8). Formation of the vinyl group suggests a ring opening pathway that results in an unsaturation at the end of the carbon chain. We rationalize this observation by the mechanism shown in Scheme 1B. The strong Lewis acid sites represented by tri-coordinated Al sites in γ-Al_2O_3 were suggested to appear more as a distorted tetrahedral ion (Scheme 1B) due to a reversible reconstruction via establishing weak bond with a nearby oxide ion [53]. It was shown that this very weak coordination bond in the strained species can be easily broken in contact with a base or an acid [53,65]. Therefore, we propose that GVL reacts with these Lewis acid (Al^+) – Lewis base (O^-) pair sites resulting in a

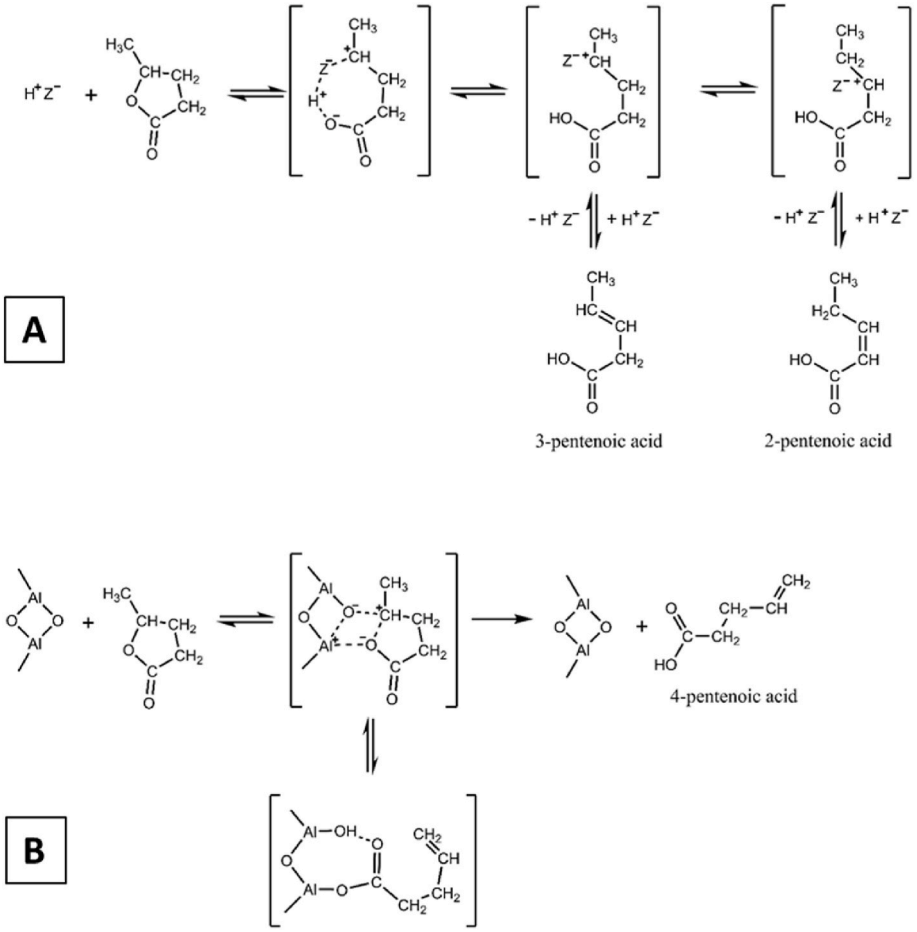

Scheme 1. Activation of GVL and formation of pentenoic acids on (A) Brønsted sites of H-zeolite and (B) Lewis acid/Lewis base pair sites of γ-Al_2O_3.

surface intermediate, in which the positively charged carbon atom of the carbenium ion intermediate is coordinated to the Lewis base (O^-) site, whereas the negatively charged oxygen atom of the broken GVL ring is coordinated to the Lewis acid (Al^+) site (Scheme 1B). Proton transfer to this latter negatively charged oxygen atom results in the formation of a carboxyl group and desorption of PE product, while the Lewis acid site becomes regenerated. The transient DRIFTS measurements revealed that monodentate surface species were formed with the involvement of Lewis acid sites. These monodentate carboxylates (Scheme 1B) can be formed via the adsorption of the PE product on the Lewis acid (Al^+) – Lewis base (O^-) pair sites; however, their formation via proton transfer to the Lewis base (O^-) sites within the adsorption complex cannot be excluded. The formation of monodentate carboxylate species was accompanied by the formation of strongly bound bidentate carboxylates due to an acid-base reaction between the carboxyl group and the basic Al-OH groups of the alumina surface (Fig. 7 and Table 3). It is important to note that introduction of cobalt hardly affected the Lewis acidity of the alumina support (Fig. 4); therefore, similar surface processes were observed on the bifunctional Co/γ-Al_2O_3 catalyst in the absence of hydrogen than on the γ-alumina support (Fig. 7 and Fig. S8).

Formation of surface carboxylates from the unsaturated carboxylic acid product was also observed on the H-Beta support most probably with the involvement of Lewis acid sites and non-acidic surface OH groups (Fig. S11). These surface processes are also observable on the bifunctional Co/H-Beta catalyst in the absence of hydrogen; however, the concentration of surface carboxylates is significantly lower than on the H-Beta support (Fig. 9). These results suggest that lattice cation cobalt in Co/H-Beta cannot form surface carboxylate with the product unsaturated carboxylic acid. The formation of surface carboxylate species proceeds also in the presence of H_2 on both bifunctional catalysts, except that these surface intermediates do not contain unsaturation in the carbon chain (Figs. 8 and 10). These results clearly suggest that the cleavage of the [CH_3CH-O] bond of the GVL molecule proceeds on the acid sites of both Co/H-Beta and Co/γ-Al_2O_3 catalysts, but the thus obtained unsaturated carboxylate species became saturated by hydrogenation.

4.2. PA and 2-MTHF selectivities

It should be noticed that although both PA and 2-MTHF products are formed on a bifunctional pathway, the activation of GVL requires different catalytic functions to get one or the other product. On the reaction route leading to PA the reaction is initiated by acid sites (Scheme 1) resulting in cleavage of the [CH_3CH-O] bond of the GVL molecule. The thus formed surface POE intermediate is hydrogenated on Co^0 particles to POA intermediate, which is then released as PA product. The overall reaction requires the uptake of one H_2 molecule. In contrast, the reaction route leading to 2-MTHF starts with the hydrogenation of the GVL carbonyl group giving 2-OH-5-MTHF. This intermediate is then transformed in a consecutive hydrogenolysis reaction to 1,4-pentanediol intermediate, which can be cyclodehydrated to 2-MTHF. The dehydration is the first acid catalyzed step of the consecutive reaction. The overall reaction requires the uptake of two H_2 molecules and release of one H_2O molecule.

Since GVL reaction is initiated either by acidic or metallic active sites, it is expected that the relative activity of these sites will determine the relative rate of the two main reaction pathways [4,18,19,23]. The Co/H-Beta and Co/γ-Al_2O_3 catalysts have catalytic functions both for ring opening and hydrogenation. High GVL conversion was attained with both catalysts at about 200 °C. However, while the Co/H-Beta catalyst was selective for PA generation, the Co/γ-Al_2O_3 catalyst showed high selectivity for 2-MTHF formation. The radically different selectivity of the catalysts under the same reaction conditions implies that factors like the acid-base strength of the catalyst also play a decisive role in controlling the relative activity and product selectivity in the two transformations. The strength of interaction between the catalyst surface and the reactant and products determines also the coverage of the active sites. The facile GVL ring opening on acid sites and subsequent formation of surface POA species starts well below 100 °C (Figs. 8 and 10), but 2-MTHF starts to appear only at around 100 °C over both catalysts (Figs. S9 and S12). The conversion to PA is determined by the adsorption-desorption equilibrium of PA chemisorption. The POA is bound more strongly to the stronger base γ-alumina than to the weaker base H-Beta zeolite. Increasing of the temperature speeds up all the reactions. However, the increase of PA desorption rate from the Co/γ-Al_2O_3 is not so steep than that of hydrogenation. The carboxylic acid product appeared in the gas phase over Co/γ-Al_2O_3 only at temperatures higher than about 250 °C (Fig. 8B and Fig. S9), whereas formation of 2-MTHF prevails at lower temperatures. On the contrary, the ring opening reaction and PA formation on the Co/H-Beta catalyst is catalyzed mainly by Brønsted acid sites, which are not blocked by carboxylate. In the lack of strong carboxylate bonding the Brønsted acid catalyzed ring opening reaction was strongly accelerated by the elevation of the reaction temperature, therefore the PA formation prevails over the Co/H-Beta catalyst even at temperature as low as 200 °C (Fig. S12).

5. Conclusions

Acid sites of γ-Al_2O_3 and zeolite H-Beta induces the ring opening of GVL at the [CH_3CH-O] bond giving pentenoate carboxylate, bound to Lewis acid sites, and pentenoic acid. Introduction of Co hardly influenced the Lewis acidity of γ-Al_2O_3, whereas the Lewis acid sites in H-Beta were partly converted to new type of Lewis acid sites represented by Co lattice cations. Over these latter sites no carboxylate species were formed, thus the concentration of surface carboxylates was significantly lower on Co/H-Beta than on the H-Beta support. The Brønsted acid sites did not take part in carboxylate formation. In the presence of hydrogenation function (Co^0) and H_2, the unsaturated carboxylate species were hydrogenated to saturated surface carboxylates, while the hydrogenation of the carbonyl group leading to intermediate of 2-MTHF formation was also initiated. The strong bonding of monodentate carboxylates to the Lewis sites of γ-Al_2O_3 prevented the acid catalyzed ring opening reaction at temperatures below about 250 °C, thus the 2-MTHF formation prevailed due to the dominating hydrogenation activity. In contrast, carboxylate formation did not block the Brønsted acid sites of H-Beta thus the ring opening reaction leading to PA formation prevailed over the hydrogenation reaction above about 175 °C.

CRediT authorship contribution statement

Gyula Novodárszki: Investigation, Data curation, Conceptualization. **Ferenc Lónyi:** Writing – review & editing, Writing – original draft, Supervision, Investigation, Funding acquisition, Formal analysis, Conceptualization. **Magdolna R. Mihályi:** Project administration, Methodology, Investigation, Data curation, Conceptualization. **Anna Vikár:** Visualization, Investigation, Data curation. **Róbert Barthos:** Investigation, Formal analysis, Data curation. **Blanka Szabó:** Visualization, Investigation, Data curation. **Jenő Hancsók:** Writing – review & editing, Conceptualization. **József Valyon:** Writing – review & editing, Conceptualization. **Hanna E. Solt:** Visualization, Validation, Methodology, Investigation, Formal analysis, Data curation.

Declaration of competing interest

The authors declare that they have no known competing financial interests or personal relationships that could have appeared to influence the work reported in this paper.

Data availability

The data that has been used is confidential.

Acknowledgements

The authors thank for the support provided by the Ministry of Innovation and Technology of Hungary from the National Research, Development, and Innovation Fund, financed under the 2019-2.1.13-TÉT_IN funding scheme (Project No. 2019-2.1.13-TÉT_IN-2020-00043).

The authors acknowledge the financial support of the project of the Economic Development and Innovation Operative Program of Hungary, GINOP-2.3.2-15-2016-00053: Development of liquid engine fuels with high hydrogen content in their molecular structures (contribution to sustainable mobility).

One of the authors (Gy. N.) thanks for the financial support provided by the Ministry for Culture and Innovation from the source of the National Research, Development and Innovation Fund, under the ÚNKP-22-4 New National Excellence Program (Eötvös Loránd University).

Abbreviations

1,4-PD	1,4-pentanediol
2-MTHF	2-methyltetrahydrofuran
2-OH-5-MTHF	2-hydroxy-5-methyltetrahydrofuran
GVL	γ-valerolactone
PA	pentanoic acid
PE	pentenoic acid
POA	pentanoate
POE	pentenoate
PPE	pentanoic acid penthylester
Py	pyridine
BET	Brunauer-Emmett-Teller method
BJH	Barett-Joyner-Halenda method
DRIFTS	Diffuse Reflectance Infrared Fourier-Transform Spectroscopy
FT-IR	Fourier-Transform Infrared Spectroscopy
H_2-TPR	Temperature-Programmed Reduction by H_2
SSA	Specific Surface Area
XRPD	X-ray Powder Diffraction

Appendix A. Supplementary data

Supplementary data to this article can be found online at https://doi.org/10.1016/j.micromeso.2023.112732.

References

[1] M.J. Climent, A. Corma, S. Iborra, Conversion of biomass platform molecules into fuel additives and liquid hydrocarbon fuels, Green Chem. 16 (2014) 516–547, https://doi.org/10.1039/c3gc41492b.
[2] R. Gérardy, D.P. Debecker, J. Estager, P. Luis, J.C.M. Monbaliu, Continuous flow upgrading of selected C2-C6 platform chemicals derived from biomass, Chem. Rev. 120 (2020) 7219–7347, https://doi.org/10.1021/acs.chemrev.9b00846.
[3] L.T. Mika, E. Cséfalvay, Á. Németh, Catalytic conversion of carbohydrates to initial platform chemicals: chemistry and sustainability, Chem. Rev. 118 (2018) 505–613, https://doi.org/10.1021/acs.chemrev.7b00395.
[4] F.M.A. Geilen, B. Engendahl, A. Harwardt, W. Marquardt, J. Klankermayer, W. Leitner, Selective and flexible transformation of biomass-derived platform chemicals by a multifunctional catalytic system, Angew. Chem. Int. Ed. 49 (2010) 5510–5514, https://doi.org/10.1002/anie.201002060.
[5] C.H. Zhou, X. Xia, C.X. Lin, D.S. Tong, J. Beltramini, Catalytic conversion of lignocellulosic biomass to fine chemicals and fuels, Chem. Soc. Rev. 40 (2011) 5588–5617, https://doi.org/10.1039/c1cs15124j.
[6] G. Novodárszki, H.E. Solt, J. Valyon, F. Lónyi, J. Hancsók, D. Deka, R. Tuba, M. R. Mihályi, Selective hydroconversion of levulinic acid to γ-valerolactone or 2-methyltetrahydrofuran over silica-supported cobalt catalysts, Catal. Sci. Technol. 9 (2019) 2291–2304, https://doi.org/10.1039/c9cy00168a.
[7] G. Novodárszki, J. Valyon, Á. Illés, S. Dóbé, D. Deka, J. Hancsók, M.R. Mihályi, Heterogeneous hydroconversion of levulinic acid over silica-supported Ni catalyst, React. Kinet. Mech. Catal. 126 (2019) 795–810, https://doi.org/10.1007/s11144-018-1507-9.
[8] I.T. Horváth, H. Mehdi, V. Fábos, L. Boda, L.T. Mika, γ-Valerolactone – a sustainable liquid for energy and carbon-based chemicals, Green Chem. 10 (2008), https://doi.org/10.1039/b712863k, 238–24.
[9] D.M. Alonso, S.G. Wettstein, J.A. Dumesic, Gamma-valerolactone, a sustainable platform molecule derived from lignocellulosic biomass, Green Chem. 15 (2013) 584–595, https://doi.org/10.1039/c3gc37065h.
[10] J.Q. Bond, D.M. Alonso, D. Wang, R.M. West, J.A. Dumesic, Integrated catalytic conversion of γ-valerolactone to liquid alkenes for transportation fuels, Science 327 (2010) 1110–1114, https://doi.org/10.1126/science.1184362.
[11] Z. Zhang, Synthesis of γ-valerolactone from carbohydrates and its applications, ChemSusChem 9 (2016) 156–171, https://doi.org/10.1002/cssc.201501089.
[12] K. Yan, Y. Yang, J. Chai, Y. Lu, Catalytic reactions of gamma-valerolactone: a platform to fuels and value-added chemicals, Appl. Catal. B Environ. 179 (2015), https://doi.org/10.1016/j.apcatb.2015.04.030.
[13] L.E. Manzer, Catalytic synthesis of α-methylene-γ-valerolactone: a biomass-derived acrylic monomer, Appl. Catal. Gen. 272 (2004) 249–256, https://doi.org/10.1016/j.apcata.2004.05.048.
[14] M. Chalid, H.J. Heeres, A.A. Broekhuis, Green polymer precursors from biomass-based levulinic acid, Procedia Chem. 4 (2012) 260–267, https://doi.org/10.1016/j.proche.2012.06.036.
[15] J.P. Lange, J.Z. Vestering, R.J. Haan, Towards "bio-based" Nylon: conversion of γ-valerolactone to methyl pentenoate under catalytic distillation conditions, Chem. Commun. (2007) 3488–3490, https://doi.org/10.1039/b705782b.
[16] F.H. Isikgor, C.R. Becer, Lignocellulosic biomass: a sustainable platform for the production of bio-based chemicals and polymers, Polym. Chem. 6 (2015) 4497–4559, https://doi.org/10.1039/c5py00263j.
[17] J.Q. Bond, D. Martin Alonso, R.M. West, J.A. Dumesic, γ-valerolactone ring-opening and decarboxylation over SiO_2/Al_2O_3 in the presence of water, Langmuir 26 (2010) 16291–16298, https://doi.org/10.1021/la101424a.
[18] J.P. Lange, R. Price, P.M. Ayoub, J. Louis, L. Petrus, L. Clarke, H. Gosselink, Valeric biofuels: a platform of cellulosic transportation fuels, Angew. Chem. Int. Ed. 49 (2010) 4479–4483, https://doi.org/10.1002/anie.201000655.
[19] G. Novodárszki, H.E. Solt, G. Lendvay, R.M. Mihályi, A. Vikár, F. Lónyi, J. Hancsók, J. Valyon, Hydroconversion mechanism of biomass-derived γ-valerolactone, Catal. Today 336 (2019) 50–62, https://doi.org/10.1016/j.cattod.2019.02.020.
[20] V. Pace, P. Hoyos, L. Castoldi, P. Domínguez De María, A.R. Alcántara, 2-Methyltetrahydrofuran (2-MeTHF): a biomass-derived solvent with broad application in organic chemistry, ChemSusChem 5 (2012) 1369–1379, https://doi.org/10.1002/cssc.201100780.
[21] J.J. Bozell, Connecting biomass and petroleum processing with a chemical bridge, Science 329 (2010) 522–523, https://doi.org/10.1126/science.1191662.
[22] H. Mehdi, V. Fábos, R. Tuba, A. Bodor, L.T. Mika, I.T. Horváth, Integration of homogeneous and heterogeneous catalytic processes for a multi-step conversion of biomass: from sucrose to levulinic acid, γ-valerolactone, 1,4-pentanediol, 2-methyl-tetrahydrofuran, and alkanes, Top. Catal. 48 (2008) 49–54, https://doi.org/10.1007/s11244-008-9047-6.
[23] V.K. Velisoju, D. Jampaiah, N. Gutta, U. Bentrup, A. Brückner, S.K. Bhargava, V. Akula, Conversion of γ-valerolactone to ethyl valerate over metal promoted Ni/ZSM-5 catalysts: influence of Ni^0/Ni^{2+} heterojunctions on activity and product selectivity, ChemCatChem 12 (2020) 1341–1349, https://doi.org/10.1002/cctc.201901966.
[24] J.Q. Bond, D. Wang, D.M. Alonso, J.A. Dumesic, Interconversion between γ-valerolactone and pentenoic acid combined with decarboxylation to form butene over silica/alumina, J. Catal. 281 (2011) 290–299, https://doi.org/10.1016/j.jcat.2011.05.011.
[25] D. Wang, S.H. Hakim, D. Martin Alonso, J.A. Dumesic, A highly selective route to linear alpha olefins from biomass-derived lactones and unsaturated acids, Chem. Commun. 49 (2013) 7040–7042, https://doi.org/10.1039/c3cc43587c.
[26] K. Kon, W. Onodera, K.I. Shimizu, Selective hydrogenation of levulinic acid to valeric acid and valeric biofuels by a Pt/HMFI catalyst, Catal. Sci. Technol. 4 (2014) 3227–3234, https://doi.org/10.1039/c4cy00504j.
[27] W. Luo, U. Deka, A.M. Beale, E.R.H. Van Eck, P.C.A. Bruijnincx, B.M. Weckhuysen, Ruthenium-catalyzed hydrogenation of levulinic acid: influence of the support and solvent on catalyst selectivity and stability, J. Catal. 301 (2013) 175–186, https://doi.org/10.1016/j.jcat.2013.02.003.
[28] P. Sun, G. Gao, Z. Zhao, C. Xia, F. Li, Stabilization of cobalt catalysts by embedment for efficient production of valeric biofuel, ACS Catal. 4 (2014) 4136–4142, https://doi.org/10.1021/cs501409s.
[29] S.N. Derle, P.A. Parikh, Hydrogenation of levulinic acid and γ-valerolactone: steps towards biofuels, Biomass Convers. Biorefinery 4 (2014) 293–299, https://doi.org/10.1007/s13399-013-0111-5.
[30] K. Yan, T. Lafleur, X. Wu, J. Chai, G. Wu, X. Xie, Cascade upgrading of γ-valerolactone to biofuels, Chem. Commun. 51 (2015) 6984–6987, https://doi.org/10.1039/c5cc01463h.
[31] T. Pan, J. Deng, Q. Xu, Y. Xu, Q.-X. Guo, Y. Fu, Catalytic conversion of biomass-derived levulinic acid to valerate esters as oxygenated fuels using supported ruthenium catalysts, Green Chem. 15 (2013) 2967–2974, https://doi.org/10.1039/c3gc40927a.
[32] R. Buitrago-Sierra, J.C. Serrano-Ruiz, F. Rodríguez-Reinoso, A. Sepúlveda-Escribano, J.A. Dumesic, Ce promoted Pd-Nb catalysts for γ-valerolactone ring-opening and hydrogenation, Green Chem. 14 (2012) 3318–3324, https://doi.org/10.1039/c2gc36161b.
[33] G.N. Yun, A. Takagaki, R. Kikuchi, S.T. Oyama, Hydrodeoxygenation of gamma-valerolactone on transition metal phosphide catalysts, Catal. Sci. Technol. 7 (2017) 281–292, https://doi.org/10.1039/c6cy02252a.
[34] J.M. Bermudez, J.A. Menéndez, A.A. Romero, E. Serrano, J. Garcia-Martinez, R. Luque, Continuous flow nanocatalysis: reaction pathways in the conversion of levulinic acid to valuable chemicals, Green Chem. 15 (2013) 2786–2792, https://doi.org/10.1039/c3gc41022f.
[35] X.L. Du, Q.Y. Bi, Y.M. Liu, Y. Cao, H.Y. He, K.N. Fan, Tunable copper-catalyzed chemoselective hydrogenolysis of biomass-derived γ-valerolactone into 1,4-

pentanediol or 2-methyltetrahydrofuran, Green Chem. 14 (2012) 935–939, https://doi.org/10.1039/c2gc16599f.
[36] I. Obregón, I. Gandarias, A. Ocio, I. García-García, N. Alvarez de Eulate, P.L. Arias, Structure-activity relationships of Ni-Cu/Al_2O_3 catalysts for γ-valerolactone conversion to 2-methyltetrahydrofuran, Appl. Catal. B Environ. 210 (2017) 328–341, https://doi.org/10.1016/j.apcatb.2017.04.006.
[37] R. Charrad, H.E. Solt, J. Valyon, L. Trif, F. Ayari, M. Mhamdi, J. Hancsók, F. Lónyi, Evaluation of Co/SSZ-13 zeolite catalysts prepared by solid-phase reaction for NO-SCR by methane, ChemistryOpen 9 (2020) 1123–1134, https://doi.org/10.1002/open.202000239.
[38] M. Mhamdi, E. Marceau, S. Khaddar-Zine, A. Ghorbel, M. Che, Y. Ben Taarit, F. Villain, Preparation of Co^{2+}/ZSM5 catalysts by solid-state reaction: influence of the precursor on cobalt speciation, Z. Phys. Chem. 219 (2005) 963–978, https://doi.org/10.1524/zpch.219.7.963.67087.
[39] V. Zholobenko, C. Freitas, M. Jendrlin, P. Bazin, A. Travert, F. Thibault-Starzyk, Probing the acid sites of zeolites with pyridine: quantitative AGIR measurements of the molar absorption coefficients, J. Catal. 385 (2020) 52–60, https://doi.org/10.1016/j.jcat.2020.03.003.
[40] C.H. Bartholomew, Hydrogen adsorption on supported cobalt, iron, and nickel, Catal. Lett. 7 (1991) 27–51, https://doi.org/10.1007/BF00764490.
[41] L.E.S. Rygh, O.H. Ellestad, P. Klæboe, C.J. Nielsen, Infrared study of CO adsorbed on Co/γ-Al_2O_3 based Fischer-Tropsch catalysts; semi-empirical calculations as a tool for vibrational assignments, Phys. Chem. Chem. Phys. 2 (2000) 1835–1846, https://doi.org/10.1039/b000188k.
[42] R.L. Chin, D.M. Hercules, Surface spectroscopic characterization of cobalt-alumina catalysts, J. Phys. Chem. 86 (1982) 360–367, https://doi.org/10.1021/j100392a016.
[43] Y. Zhang, H. Xiong, K. Liew, J. Li, Effect of magnesia on alumina-supported cobalt Fischer-Tropsch synthesis catalysts, J. Mol. Catal. Chem. 237 (2005) 172–181, https://doi.org/10.1016/j.molcata.2005.04.057.
[44] W.-J. Wang, Y.-W. Chen, Influence of metal loading on the reducibility and hydrogenation activity of cobalt/alumina catalysts, Appl. Catal. 77 (1991) 223–233, https://doi.org/10.1016/0166-9834(91)80067-7.
[45] G. Jacobs, W. Ma, B.H. Davis, Influence of reduction promoters on stability of cobalt/γ-alumina Fischer-Tropsch synthesis catalysts, Catalysts 4 (2014) 49–76, https://doi.org/10.3390/catal4010049.
[46] X. Wang, H. Chen, W.M.H. Sachtler, Selective reduction of NO_x with hydrocarbons over Co/MFI prepared by sublimation of $CoBr_2$ and other methods, Appl. Catal. B Environ. 29 (2001) 47–60, https://doi.org/10.1016/S0926-3373(00)00186-7.
[47] A.Y. Khodakov, J. Lynch, D. Bazin, B. Rebours, N. Zanier, B. Moisson, P. Chaumette, Reducibility of cobalt species in silica-supported Fischer-Tropsch catalysts, J. Catal. 168 (1997) 16–25, https://doi.org/10.1006/jcat.1997.1573.
[48] G. Jacobs, Y. Ji, B.H. Davis, D. Cronauer, A.J. Kropf, C.L. Marshall, Fischer-Tropsch synthesis: temperature programmed EXAFS/XANES investigation of the influence of support type, cobalt loading, and noble metal promoter addition to the reduction behavior of cobalt oxide particles, Appl. Catal. Gen. 333 (2007) 177–191, https://doi.org/10.1016/j.apcata.2007.07.027.
[49] P. Arnoldy, J.A. Moulijn, Temperature-programmed reduction of $CoOAl_2O_3$ catalysts, J. Catal. 93 (1985) 38–54, https://doi.org/10.1016/0021-9517(85)90149-6.
[50] A. Lapidus, A. Krylova, V. Kazanskii, V. Borovkov, A. Zaitsev, J. Rathousky, A. Zukal, M. Jančálková, Hydrocarbon synthesis from carbon monoxide and hydrogen on impregnated cobalt catalysts Part I. Physico-chemical properties of 10% cobalt/alumina and 10% cobalt/silica, Appl. Catal. 73 (1991) 65–81, https://doi.org/10.1016/0166-9834(91)85113-A.
[51] N. Sheppard, T.T. Nguyen, The vibrational spectra of carbon monoxide on the surfaces of metal catalysts – a suggested scheme of interpretation, in: R.J.H. Clark, R.E. Hester (Eds.), Advances in Infrared and Raman Spectroscopy", vol. 5, HEYDEN, 1978. Ch. 2.
[52] F. Geobaldo, B. Onida, P. Rivolo, F. Di Renzo, F. Fajula, E. Garrone, Nature and reactivity of Co species in a cobalt-containing beta zeolite: an FTIR study, Catal. Today 70 (2001) 107–119, https://doi.org/10.1016/S0920-5861(01)00411-4.
[53] G. Busca, The surface of transitional aluminas: a critical review, Catal. Today 226 (2014) 2–13, https://doi.org/10.1016/j.cattod.2013.08.003.
[54] I. Kiricsi, C. Flego, G. Pazzuconi, W.O. Parker, R. Millini, C. Perego, G. Bellussi, Progress toward understanding zeolite β acidity: an IR and ^{27}Al NMR spectroscopic study, J. Phys. Chem. 98 (1994) 4627–4634, https://doi.org/10.1021/j100068a024.
[55] A. Bellmann, H. Atia, U. Bentrup, A. Brückner, Mechanism of the selective reduction of NO_x by methane over Co-ZSM-5, Appl. Catal. B Environ. 230 (2018) 184–193, https://doi.org/10.1016/j.apcatb.2018.02.051.
[56] L.J. Bellamy, The Infrared Spectra of Complex Molecules", third ed., Chapman and Hall, London, 1975. Part 1, Ch. 3.
[57] P. Larkin, Infrared and Raman Spectroscopy; Principles and Spectral Interpretation, Elsevier, 2011. https://www.elsevier.com/books/infrared-and-raman-spectroscopy/larkin/978-0-12-386984-5.
[58] N. Scotti, M. Dangate, A. Gervasini, C. Evangelisti, N. Ravasio, F. Zaccheria, Unraveling the role of low coordination sites in a Cu metal nanoparticle: a step toward the selective synthesis of second generation biofuels, ACS Catal. 4 (2014) 2818–2826, https://doi.org/10.1021/cs500581a.
[59] A. Vikár, H.E. Solt, G. Novodárszki, M.R. Mihályi, R. Barthos, A. Domján, J. Hancsók, J. Valyon, F. Lónyi, A study of the mechanism of triglyceride hydrodeoxygenation over alumina-supported and phosphatized-alumina-supported Pd catalysts, J. Catal. 404 (2021) 67–79, https://doi.org/10.1016/j.jcat.2021.08.052.
[60] H.E. Evans, W.H. Weinberg, A comparison of the vibrational structures of ethanol, acetic acid, and acetaldehyde adsorbed on alumina, J. Chem. Phys. 71 (1979) 4789–4798, https://doi.org/10.1063/1.438317.
[61] J. Van Den Brand, O. Blajiev, P.C.J. Beentjes, H. Terryn, J.H.W. De Wit, Interaction of ester functional groups with aluminum oxide surfaces studied using infrared reflection absorption spectroscopy, Langmuir 20 (2004) 6318–6326, https://doi.org/10.1021/la049456a.
[62] J.E. Tackett, FT-IR characterization of metal acetates in aqueous solution, Appl. Spectrosc. 43 (1989) 483–489, https://doi.org/10.1366/0003702894202931.
[63] A.S. Milev, G.S. Kamali Kannangara, M.A. Wilson, Template-directed synthesis of hydroxyapatite from a lamellar phosphonate precursor, Langmuir 20 (2004) 1888–1894, https://doi.org/10.1021/la0355601.
[64] A.R. Barron, The interaction of carboxylic acids with aluminium oxides: journeying from a basic understanding of alumina nanoparticles to water treatment for industrial and humanitarian applications, Dalton Trans. 43 (2014) 8127–8143, https://doi.org/10.1039/c4dt00504j.
[65] E. Decanio, J.W. Bruno, V.P. Nero, J.C. Edwards, ^{27}Al NMR, FT-IR and Ethanol-^{18}O TPD characterization of fluorided alumina, J. Catal. 140 (1993) 84–102, https://doi.org/10.1006/jcat.1993.1070.